Development of Cookstove Emissions and Performance Testing Suite with Time-resolved Particulate Matter Analysis and Excess Air Estimation

Benjamin Sullivan

A thesis submitted in partial fulfillment of the requirements for the degree

Master of Science in Mechanical Engineering

University of Washington

2016

Committee:

Jonathan Posner, Co-Chair

John Kramlich, Co-Chair

Ashley Emery

Paul Means

Program Authorized to Offer Degree:

Department of Mechanical Engineering

University of Washington

Abstract

Development of Cookstove Emissions and Performance Testing Suite with Time-resolved Particulate Matter Analysis and Excess Air Estimation

Benjamin Sullivan

Chairs of the Supervisory Committee:

Associate Professor Jonathan Posner
Professor John Kramlich
Department of Mechanical Engineering

Biomass combustion results in 4.3 million premature deaths annually due to indoor air pollution, and contributes significantly to global greenhouse gas emissions and deforestation. The majority of biomass combustion for cooking and heating is done with rudimentary stoves which are inefficient and produce harmful emissions. Improved cookstoves offer a cleaner and more efficient alternative. The design and testing of improved cookstoves requires a sophisticated testing suite to fully characterize stove performance. In this thesis, the design and development of a cookstove emissions and performance testing suite are detailed, with the novel additions of time-resolved particulate matter (PM) analysis and excess air estimation. Time-resolved cookstove emissions monitoring of particulate matter less than 2.5 μm in diameter ($PM_{2.5}$) are made using a Tapered Element Oscillating Microbalance (TEOM) system. Significant modification and calibration of the TEOM system is presented to bring it into agreement with the standard gravimetric filter method. The real-time measurement system is able to correlate operator actions/operating conditions, specifically during refueling and lighting phases, with transient high $PM_{2.5}$ events in a wood side-fed natural draft stove. I develop a protocol for

estimating the amount of excess air in a cookstove and use it to analyze the amount of excess air present in a wood side-fed natural draft stove with and without a feed door. The cookstove used is found to have a significant amount of excess air present, though the addition of a feed door reduces this. Experimental uncertainties of cookstove performance and emissions testing suite are calculated for individual components as well as global comparison metrics.

Table of Contents

List of Figures

List of Tables

Acknowledgements

This research was funded by the United States Department of Energy through grant DE-EE0006284.

In the two years over which this work was performed, I was supported by a large number of mentors, colleagues, and friends, and it is my pleasure to acknowledge them and their contributions.

First, I would like to thank my two primary advisors, Jonathan Posner and John Kramlich for their support. I sincerely appreciate the learning opportunities that were presented, and the patience and mentorship that was shown to me. I believe that my skill as a researcher and communicator is a direct reflection of the advice and lessons that I've learned from you.

I am grateful to the additional members of my Thesis Committee, Ashley Emery and Paul Means, who provided me with enriching conversations and advice. Thank you for pointing me in the right direction in many of the struggles and barriers that I faced throughout this work.

Thank you to all of those at BURN Design Lab, who aided in the construction and design of many pieces on this work. I truly value all of your expertise, and appreciate the patience you showed as this project was just beginning.

I would also like to acknowledge my labmates in the Cookstove Research Group at the University of Washington. I appreciate the countless discussions that we had, and the willingness to help without question. My experience would not have been the same without Garrett Allawatt, Anamol Pundle, Devin Udesen, and Jackson McFall. Thank you for your continuous support.

Finally, I dedicate this thesis to my parents, Gregory and Deanie Sullivan, who instilled on me the curiosity and drive needed to achieve my goals. Thank you for your constant advice and unconditional love. I could not have reached this point without you. Thank you.

Chapter 1: Significance and Background

This chapter provides motivation for the work presented and the need for continued development of cookstoves. To successfully design innovative cookstoves, rigorous testing methodologies and testing suites are required to quantify stove performance and compare competing morphologies. Current testing methodologies for cookstove comparison testing are discussed in this section. The detailed testing protocols are not the only methodologies used to evaluate cookstove performance, though they are the most commonly used. The required equipment for cookstove emissions monitoring and performance testing are discussed in the context of two previously described cookstove comparison testing systems. Various methodologies for particulate matter analysis are also described.

1.1 Significance

There are nearly 3 billion people dependent on wood, coal, and other biomass wastes for their cooking and heating needs (Bonjour et al. 2013). The vast majority of this fuel is used in an open fire (Hutton et al. 2007). Indoor air pollution caused by solid fuel combustion leads to deleterious health effects such as lung cancer, chronic obstructive pulmonary disease, and other lower respiratory tract infections, and these disproportionately affect underdeveloped and developing regions (Ezzati & Kammen 2001). This pollution is responsible for 7.7% of the global burden of disease and 4.3 million premature deaths annually (World Health Organization 2014). Residential solid fuel burning also results in significant greenhouse gas emissions, producing up to 25% of global black carbon (BC) emissions (Bond et al. 2004), which contributes roughly 2,200 times more to global warming than CO_2 on a per-mass basis (Bond & Sun 2005). This effect on global climate change is compounded by the fact that wood consumption for cooking and heating needs contributes significantly to deforestation (Baldwin 1986).

Improved cookstoves have been introduced in developing countries to combat these harmful impacts, with the main goals of increasing thermal efficiency and decreasing emissions, especially particulate matter that is less than 2.5 microns in diameter ($PM_{2.5}$). $PM_{2.5}$ is especially harmful compared to larger particles (Schwartz et al. 1996), as the small diameter allows the particles to penetrate deeper into the lungs, which makes expelling the particles more difficult for the body. Traditional open fires (three-stone fires), which are the main option for nearly 3 billion people (Hutton et al. 2007), have typical thermal efficiencies of 14-15% and $PM_{2.5}$ emissions of 700-1400 $mg/MJ_{delivered}$ (Jetter et al. 2012). Commercially available natural draft cookstoves have thermal efficiencies near 35% and $PM_{2.5}$ emissions of ~ 500 $mg/MJ_{delivered}$ (Jetter et al. 2012). While the thermal efficiencies are approaching 40-45% (Kshirsager & Kalamkar 2014) and PM emissions are drastically reduced by improved cookstoves (McCracken & Smith 1998; Masera et al. 2007; MacCarty et al. 2010), PM emissions are still well above the World Health Organization's (WHO) recommended $PM_{2.5}$ exposure guidelines (0.035 mg/m^3) (World Health Organization 2006). In a recent study of improved cookstove implementation in India and Mexico, measured indoor $PM_{2.5}$ concentrations after cookstove introduction (0.33 mg/m^3) were still nearly ten times the WHO $PM_{2.5}$ guideline levels. (Smith et al. 2007) There remains a significant amount of work and innovation required to develop cookstoves that comply with the WHO $PM_{2.5}$ standards. To aid in cookstove design and development, a thorough testing methodology is required that quantitatively characterizes cookstove performance to compare competing stove designs and morphologies, as well as time-resolved diagnostics to better understand cookstove dynamics that lead to good or bad cookstove performance..

1.2 Objectives

The objectives of this thesis are to design, construct, and validate a complete cookstove testing system that can quantify cookstove performance and emissions to aid in cookstove design and development, to design, implement, and validate a time-resolved gravimetric $PM_{2.5}$

measurement system for cookstove emissions monitoring and to investigate $PM_{2.5}$ production during different portions of typical cookstove operation, to develop a protocol to experimentally estimate the amount of excess air present in natural draft cookstoves, and to calculate the inherent experimental uncertainty associated with the detailed testing apparatus in the context of standardized cookstove comparison metrics. The work presented here is designed to aid cookstove designers in better understanding cookstove operation and characteristics by describing the design of a comprehensive cookstove testing suite and the introduction of several novel cookstove analysis tools, namely a time-resolved gravimetric $PM_{2.5}$ analyzer and a protocol for estimating the amount of excess air present during cookstove operation. By better understanding cookstove dynamics, cookstove designers can develop cleaner and more efficient cookstoves.

1.3 ISO/IWA Cookstove Comparison Metrics

The International Organization for Standardization has developed a set of comparison metrics for quantitative cookstove evaluation. These are detailed in *ISO/IWA 11:2012 Guidelines for evaluating cookstove performance* (ISO 2012). The metrics are separated into three groupings: cookstove emissions, thermal efficiency/fuel use, and indoor emissions. While the cookstove emissions and indoor emissions categories are very similar, the two groupings use different units to describe emissions rates, providing unique information about stove performance. Each metric has five tiers (0-4, with Tier 4 being the most stringent). The metrics and tiers are listed in Table 1 and Table 2. The high and low power metrics denote the boil and simmer phase of the Water Boil Test, detailed in Chapter 1.4.1.

Table 1: ISO/IWA Tiers for emissions

	High Power CO (g/MJ_d)	Low Power CO (g/min/L)	High Power $PM_{2.5}$ ($mg/(MJ_d)$	Low Power $PM_{2.5}$ (mg/min/L)
Tier 0	> 16	> 0.2	> 979	> 8
Tier 1	≤ 16	≤ 0.2	≤ 979	≤ 8
Tier 2	≤ 11	≤ 0.13	≤ 386	≤ 4
Tier 3	≤ 9	≤ 0.10	≤ 168	≤ 2
Tier 4	≤ 8	≤ 0.09	≤ 41	≤ 1

Table 2: ISO/IWA Tiers for thermal efficiency/fuel use and indoor emissions

	High Power Thermal Efficiency (%)	Low Power Specific Consumption (MJ/min/L)	Indoor Emissions CO (g/min)	Indoor Emissions $PM_{2.5}$ (mg/min)
Tier 0	< 15	> 0.050	> 0.97	> 40
Tier 1	≥ 15	≤ 0.050	≤ 0.97	≤ 40
Tier 2	≥ 25	≤ 0.039	≤ 0.62	≤ 17
Tier 3	≥ 35	≤ 0.028	≤ 0.49	≤ 8
Tier 4	≥ 45	≤ 0.017	≤ 0.42	≤ 2

MJ_d denotes the energy delivered to the water in the pot.

The ISO/IWA tiers are designed to operate using the Water Boil Test (WBT) 4.2.3, which is detailed in Chapter 1.4.1. The high power and low power metrics are designed to characterize stove performance as the user transitions from heating the food/water as fast as possible (in the case of boiling water for tea, for example) to a simmer mode, in which the user is only trying to maintain the food/water temperature. The cookstove community has found that the carbon monoxide metrics are relatively easy to meet, while the thermal efficiency/fuel use and PM

emissions are more difficult. The $PM_{2.5}$ and CO indoor emissions metrics are included for straightforward comparison against the World Health Organization's (WHO) intermediate household combustion emissions rate targets of 1.75 mg/min and 0.35 g/min for PM and CO respectively (World Health Organization 2014). The final WHO emissions rate targets are 0.23 mg/min (PM) and 0.16 g/min (CO) (World Health Organization 2014).

1.4 Existing Testing Methodologies

Three of the most common testing methodologies for evaluating cookstove performance are the Water Boil Test (WBT), the Controlled Cooking Test (CCT), and the Kitchen Protocol Test (KPT). These tests attempt to represent in-field conditions while maintaining reproducibility and testing ease. Laboratory tests have been found to report significantly lower incomplete combustion products (Johnson et al. 2008) and particulate matter (Roden et al. 2009) emissions when compared to field tests. It was also found that laboratory tests do not reproduce high-emissions events typically seen in in-field tests (Chen et al. 2012). The laboratory protocols also produce higher thermal efficiencies than are found in field tests (Manibog 1984). These discrepancies may be due to inappropriate laboratory operating conditions, such as lower firepowers, different fire-starting technique, as well as discrepancies in fuel quality, size, or loading practices (Chen et al. 2012). Field testing is, however, very expensive and labor-intensive, and this makes it more difficult to use during stove design and prototyping. In-field testing is inherently more inconsistent compared to laboratory tests due to the number of uncontrollable variables, such as fuel quality and user actions. Field testing is often conducted in challenging locations as well, making comprehensive stove characterization difficult (Berrueta et al. 2008). It is important to note that operating conditions in laboratory tests can be chosen to result in better cookstove performance, and that these results may not be representative of in-field operation. Standardized testing protocols should be used as a guide with a broad spectrum of operating conditions to fully

characterize cookstove performance. This section briefly reviews WBT, KPT, and CCT protocols, as well as the necessary equipment.

1.4.1 Water Boil Test (WBT) Version 4.2.3

The Water Boil Test (Global Alliance for Clean Cookstoves 2014a) is the most commonly used cookstove comparison test, developed by Engineers in Technical and Humanitarian Opportunities of Service (ETHOS), the Partnership for Clean Indoor Air (PCIA), and The Global Alliance for Clean Cookstoves. It is a laboratory procedure, meant to produce controlled and repeatable results for cookstove evaluation. The test is split into three distinct sections: cold-start, hot-start, and simmer. Hot-start is considered optional. In cold-start, the cookstove starts at room temperature, and 5 liters of water in a typical pot (defined as typical for the region of interest) is heated to the boiling temperature. All stove emissions are captured by an emissions hood, from which CO and $PM_{2.5}$ are extracted for analysis. The mass of the wood required to bring the water to a boil is also recorded. The cold-start section ends once the water reaches the local boiling temperature. The boiling water is then poured out and a fresh 5 liters of water is added to the pot for the hot-start (if hot-start is desired). The process is repeated with all of the same metrics recorded. Once the water reaches the boiling temperature after the hot/cold start, the water is kept near the boiling temperature (± 5°C) for 45 minutes during the simmer phase. Again, the emissions are characterized, and the mass of wood required is recorded. The ISO/IWA tiers detailed in Chapter 1.3 are then calculated for universal comparison.

There are several limitations and potential sources of inaccuracy when using the WBT and associated ISO/IWA tiers. Controlling the effects of water evaporation remains a hurdle for the WBT. During the weighing procedures between the boil and simmer phases, a significant amount of water can be lost to evaporation if the weighing is not done in a timely manner due to delay after the boiling temperature is reached. This results in an over-calculation of Low Power CO,

Low Power PM, and Low Power Specific Consumption due to the lower mass of water in the denominator of these metrics.

The rate of evaporation in the boil phase also affects metrics in the simmer phase. Simmer metrics are dependent on the mass of water present at the end of the simmer portion of the test, which is dependent on the water mass at the end of boil, as this sets the starting mass for the simmer portion. The mass of water lost to evaporation during the simmer phase is roughly fixed, as the temperature of the water and the simmer time are specified. This results in a direct relationship between the mass of water remaining at the end of boil and the mass of water remaining at simmer. Cookstoves that are able to boil the water more quickly in the boil phase lose less water to evaporation, and start the simmer phase with more water compared to a stove with a slow time to boil. This results in a larger denominator (due to the increase in the amount of water present) in the low power metrics, improving results. Whether by design or not, this dependency rewards cookstoves with a high turn-down ratio which are able to boil water very quickly.

L'orange *et al*. (2012) argued for several modifications to the WBT, such as the addition of a pot lid to reduce the complications associated with water evaporation, as well as a lower end temperature for the boil phase. Currently, the WBT dictates the end of the boil phase as the local boil temperature. This can lead to testing inconsistencies between locations, as well as increased variation within a single testing facility due to evaporative losses. By selecting an end temperature below the boil temperature (L'orange et al. argue for a 90 °C end temperature), the coefficient of variation can be decreased by 4 times (L'orange et al. 2012). This also results in more comparable times to boil.

Pot selection can also significantly affect cookstove performance. The WBT specifies that a pot typical of the region of interest should be used, though there is often a great deal of variability even within a single region. The determination of what is typical is left to the researcher. Pot

selection can also affect the amount of water used during testing. Pots with a larger diameter have a larger water surface area, resulting in an increase in evaporative losses over the duration of the test, affecting simmer phase metrics as previously described.

The Water Boil Test allows for a great deal individual interpretation, allowing operating conditions to be optimized to maximize cookstove performance. While these operating conditions should be recorded, in practice only the tiered comparison metrics are publicized and compared. This results in a potential disconnect between laboratory testing results and in-field results.

1.4.2 Controlled Cooking Test (CCT) Version 2.0

The Controlled Cooking Test (Global Alliance for Clean Cookstoves 2004) is designed to more accurately reproduce real-world practice. The CCT is also a laboratory procedure. The main difference between the CCT and the WBT is that the CCT uses a standardized cooking task as the ending criteria, as opposed to the WBT which uses boiling water. Researchers are encouraged to gather user input to determine what a standard cooking task might be, which is often unique to the region of interest. During testing, the test meal is cooked as it is in-field. No emissions data are collected, with the majority of emphasis placed on efficiency metrics. The end weight of the food is recorded, as well as the amount of required wood. The specific fuel consumption (g_{fuel}/kg_{food}) is calculated, and compared to the baseline cookstove. The time required to complete the cooking task is also a comparison metric. The current CCT protocol does not require emissions collection or comparison. The CCT is not a universal comparison test, as there is no globally accepted cooking task. Instead, the CCT is useful for two-stove direct comparisons. The CCT may be more representative of actual in-field stove usage than more standardized laboratory procedures such as the WBT, as cooking a typical meal may restrict operating conditions such as firepower or time, potentially lowering the occurrence of optimized conditions to maximize performance. There is still a great deal of individual interpretation, however, and is subject to many of the same interpretation issues as the WBT.

1.4.3 Kitchen Protocol Test (KPT) Version 3.0

The Kitchen Protocol Test (Global Alliance for Clean Cookstoves 2007) is a field test that aims to quantify fuel consumption on a per person basis and the effect of improved cookstove introduction. Users in the target population are recruited to cook as they normally would, using an improved cookstove. The test is conducted over several days, with the amount of fuel and the number individuals provided for using the cookstove. A separate session of testing is conducted prior to the introduction of the cookstove to establish a baseline fuel usage. There is no set procedure, as actual users are asked to cook as they would regularly. Metrics (mass of fuel consumed) are compared on a per person basis (kg_{fuel}/person). The benefit of the KPT is that it fully captures in-field cookstove use. However, the KPT is not a universal comparison test, but can be helpful in determining how improved cookstoves might benefit the end users. The KPT can also be prohibitively expensive to conduct and often requires many months of planning to ensure successful field tests. The current KPT protocol makes no recommendations for emissions collection or comparison.

1.5 Existing Cookstove Emission and Performance Testing Systems

There are several cookstove emission and performance monitoring systems that have been described in the literature. The systems detailed below are designed for laboratory tests, such as the WBT. There are also a number of alternative testing systems designed for field use, generally based on sampling rakes/probes or mobile emissions hoods. Rakes/probes are typically constructed from radial metal tubes with sample ports throughout the “arms” to fully characterize the emissions plume from the cookstoves (Roden et al. 2009; Johnson et al. 2010). Mobile emissions hoods are placed over cookstoves to capture all of the emissions which are then analyzed in a similar manner to laboratory procedures (Johnson et al. 2008; MacCarty et al. 2008).

Two of the most thoroughly described laboratory testing systems are the Laboratory Emissions Monitoring System (LEMS) (Aprovecho Research Center 2013) and the testing suite used by Jetter et al. (2012). The LEMS is a commercially available laboratory cookstove testing system by Aprovecho Research Center (Cottage Grove, OR). The testing suite used by Jetter et al. was custom built. Both allow for complete testing of cookstoves through the WBT protocol, though lab-based CCT tests are also possible. Both systems consist of an emissions hood and ducting, with the flow through the hood and ducting driven by a blower before being exhausted outside of the laboratory. The air flow rates through the ducting are adjustable to ensure that the bulk flow does not impact stove performance. This is especially important when testing natural draft stoves, as an increased hood face velocity may cause the cookstove to operate in a pseudo-forced draft regime. The LEMS system uses a non-dispersive infrared (NDIR) analyzer (GC-0011, COZIR) to measure CO_2 concentration, and a solid-state CO sensor (CO-AF, AlphaSense, Great Notley, United Kingdom) to measure CO concentrations. Solid state sensors use an electrochemical reaction in which the target gas reacts with an electrolyte in the sensor and produces a current. These sensors are less expensive than NDIR by as much as 10 times, though suffer from temperature sensitivity, though this response can be modeled and corrected for, slow response time (on the order of 30 seconds), and require frequent recalibrations due to increased drift (Aleixandre & Gerboles 2012). NDIR sensors rely on the difference in absorption spectrum between gases. The sensors emit an infrared beam at a specific wavelength for the target gas and measure the amount of transmitted infrared light. The concentration of the target gas is then calculated using the Beer-Lambert Law: $I = I_0 e^{-KLC}$, where I is the intensity of light in the target gas, I_0 is the intensity in a reference gas, such as nitrogen or argon, K is a factor dependent on the target gas, L is the path-length between the light source and detector, and C is the concentration of the target gas. NDIR sensors are very accurate and can operate for long periods of time without recalibration (Pandey & Kim 2007). The Jetter system uses a two-component

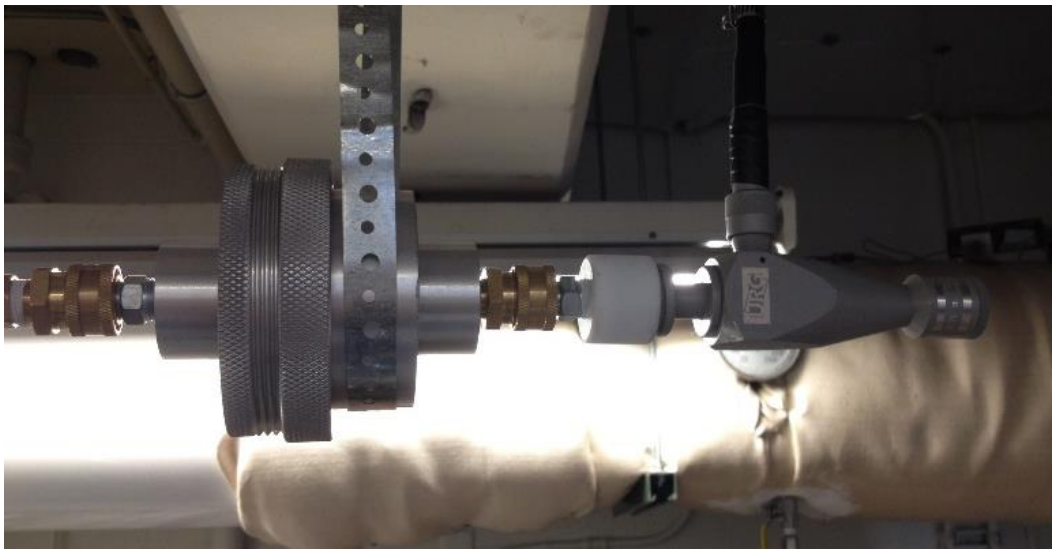

Figure 1: Gravimetric filter housing (left) and $PM_{2.5}$ cyclone (right). The pre-dried pre-weighed filters are placed in the filter housing. Once the test begins, the vacuum pump (not pictured) is turned on. Particles collect on the filter, and once the test is completed, the pump is turned off and the filter is removed, dried, and weighed. The differential mass on the filter is then calculated for the test. While a cyclone is not required for gravimetric filter operation, cookstove comparison metrics are based on $PM_{2.5}$, so a cyclone is required.

NDIR analyzer for both CO_2 and CO concentrations (Models 200, California Analytical Instruments, Orange, CA). To measure $PM_{2.5}$, the LEMS system uses two systems: a scattering photometer/nephelometer to estimate real-time $PM_{2.5}$ concentrations during a test and a gravimetric filter method in which a filter is weighed before and after each test to measure the total mass of $PM_{2.5}$ produced. The Jetter suite uses a similar gravimetric system. The differences between various particulate matter analyzers are discussed in more detail in Chapter 1.6.

1.6 Particulate Matter Analyzers

There are a number of available methods to analyze PM production. While this is not an exhaustive list, the methods most widely used in cookstove analysis are detailed.

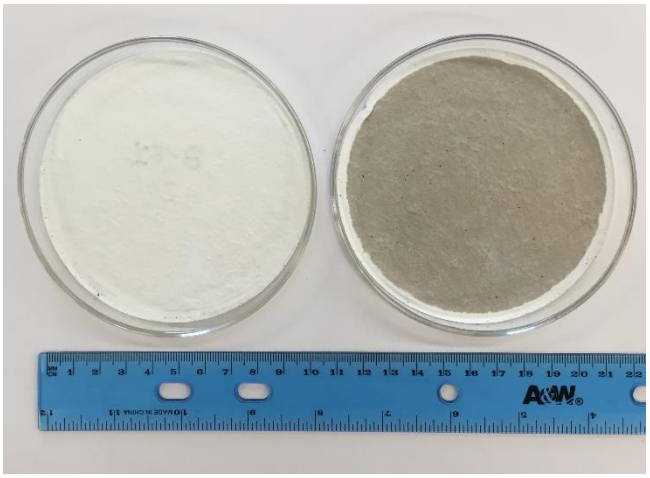

Figure 2: 102 mm borosilicate filters. The left filter is unused and the right filter is shown after 10 minutes of a cookstove comparison test. The filters are inserted into the filter housing after being desiccated/oven-dried and weighed. They are then removed after the testing is completed, desiccated/oven-dried, and weighed again to calculate the mass deposited.

1.6.1 Gravimetric Filter Method

The gravimetric filter method is one of the most often used methods for cookstove analysis. It is considered highly accurate due to its simplicity and its direct measurement of mass. In this method, a pre-dried, pre-weighed filter is placed into a filter housing, shown in Figure 1, and the sample gas is drawn through the filter housing by a vacuum pump. The filters are comprised of glass fibers (borosilicate). If only particles smaller than a certain diameter are required, such as in the case of cookstove analysis where only particles less than 2.5 microns in diameter are measured, a cyclone can be added before the filter housing. All particles larger than the aerodynamic cutoff point are discarded by the cyclone, while particles less than the cutoff are allowed to pass through. The flow rate through the assembly is controlled by a sized critical orifice located between the filter housing and vacuum pump. Particles collect on the filter and once the

test is completed, the filter is removed and desiccated. The filter can be desiccated for 24 hours or alternatively oven dried at 104°C for 2-3 hours (Method 5, United States Environmental Protection Agency n.d.). If there are semi-volatile/volatile compounds present in the sample, the filter should be desiccated to avoid any undesirable mass loss, depending on the compounds of interest. The filter is then weighed again to determine the differential mass. Sample filters used in a gravimetric system are shown in Figure 2.

The USEPA's Method 5 (United States Environmental Protection Agency n.d.) is the standard procedure for gravimetric filter analysis. While gravimetric methods are considered the comparison standard, these methods are laborious for researchers to perform and results can lag behind tests by a day or more because of the time required to dry the filters before the final weighing. Gravimetric methods only provide the total PM mass produced over the entire test, and thus cannot be used to provide time-resolved PM production. They are, however, considered the most accurate means of measuring PM concentrations.

1.6.2 Optical Methods

Optical methods, such as nephelometry, can be used to determine instantaneous particle concentrations of a sample. Nephelometry measures particle concentrations by collecting light scattered from particles illuminated by a laser beam. For particles with a diameter of less than 10% of the laser wavelength used (λ), Rayleigh theory describes the scattering behavior. At these small particle diameters, the light scattering is front-back symmetric, with minimums of intensity at 90° relative to the incident light (Hahn 2004). The total scattering cross section is given by Equation 1.

$$\sigma_{scattering} = \frac{2\lambda^2}{3\pi}\left(\frac{2\pi a}{\lambda}\right)^6 \left|\frac{m^2-1}{m^2+2}\right|^2 \qquad \text{Eq. 1}$$

Where λ is the wavelength of light used, a is the particle diameter, and m is the refractive index. The scattering is proportional to the diameter of the particle raised to the sixth power.

At larger diameters, the Mie theory correctly describes scattering behavior. The total scattering cross section is given by Equation 2.

$$\sigma_{scattering} = \frac{\lambda^2}{8\pi^2}(i_1 + i_2) \qquad \text{Eq. 2}$$

Where i_1 and i_2 are intensity functions calculated separately. The scattering caused by particles described by Mie theory is dependent on the angle of incident light (Hahn 2004).

Nephelometry provides continuous particle concentration data, which can be integrated over the test to give a measure of the total mass produced during a test. Optical systems are also relatively easy to implement. Light scattering methods require the use of calibrated scattering coefficients to correlate the amount of scattered light to particle size. These are unique to the particle type and are highly dependent on particle chemistry, shape, size, and density which can result in a variance of ±30% mass concentrations (Molenar 2005). The light flux measured by the photodetector for a given sample is given by Equation 3 (Thomas & Gerbhart 1994):

$$P = I_0 V_m C \int_0^n f(d) S(d, m, \lambda) \partial d \qquad \text{Eq. 3}$$

Where I_0 is the illumination intensity, V_m is the sensing volume, C is the number concentration, $f(d)$ is the size distribution function for the particle sample, $S(d, m, \lambda)$ is the light flux scattered by a single particle, and m and λ are the refractive index of the particles and the wavelength of light used, respectively. As P varies, it becomes very difficult to determine which of the input variables (number concentration C, refractive index m, or size distribution $f(d)$) have changed, leading to measurement uncertainty. Some cookstove testing systems such as the LEMS use optical measuring methods in conjunction with gravimetric methods to provide semi-quantitative time-

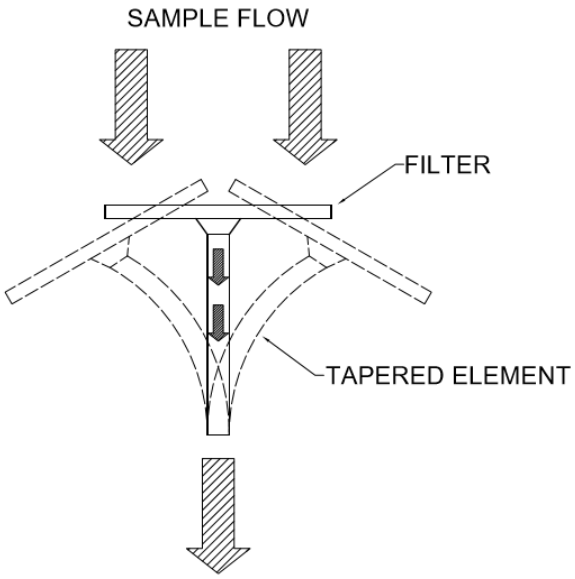

Figure 3: TEOM system theory of operation (exaggerated). The cantilevered filter oscillates at its natural frequency, which in continually monitored. The sample flow (perpendicular to the filter) is drawn through the filter and through the tapered element. As mass accumulates on the filter, the oscillation frequency changes, and the change in mass is then calculated.

resolved particle concentration data (measured by a nephelometer) alongside total mass produced (measured by the gravimetric filter). Side-by-side tests such as this also provide correlation points against which the nephelometer can be calibrated. Nephelometry provides some qualitative information on major sooting events during a burn, though there is a great deal of uncertainty in the measurements and it is questionable if nephelometry can be used as a quantitative measurement strategy for evaluating improved cookstove performance.

Figure 4: ThermoScientific TEOM 1405 system. The oscillating filter assembly is located in the lockbox on the right. The data output screen and interface is located to the left.

1.6.3 Tapered Element Oscillating Microbalance

The tapered element oscillating microbalance (TEOM) is a system that has traditionally been used for long-term ambient air monitoring of $PM_{2.5}$. It allows for time-resolved particulate matter concentration and total mass measurement. TEOM systems measure the particle concentration using a filter on a cantilevered tapered element that oscillates at its natural frequency. The sample flow with entrained particles flows through the filter and down the tapered element, depositing the particles onto the filter. As the particulate matter accumulates on the filter, the natural oscillation frequency changes, and the change in mass is calculated using $\Delta m = K_0 * \left(\frac{1}{f_1^2} - \frac{1}{f_0^2}\right)$ where K_0 is

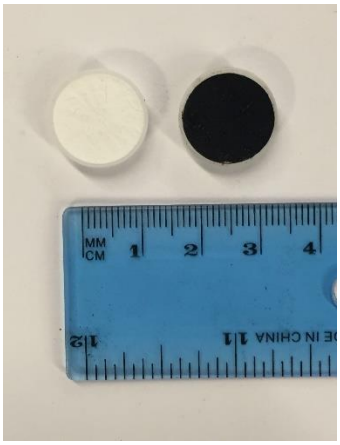

Figure 5: TEOM filters, clean (left) and used (right). The used filter was placed in the TEOM for several weeks' worth of tests. The filters are placed on the oscillating tapered element. As mass is accumulated on the filters, the tapered element/filter system oscillates at a slower frequency. This change in frequency is used to calculate the accumulated mass.

the factory set calibration constant, and f_0 and f_1 are the respective measured frequencies of the filter at some initial time and some time later (ThermoFisher Scientific 2008). As the flow rate through the filter is known (set at 3 L/min), the average mass concentration ($\mu m/m^3$) over the period of sampling can be calculated. The mechanism of TEOM operation is shown in Figure 3. In this work (discussed in Chapter 3) we use a 1405 TEOM (ThermoScientific, Waltham, MA), pictured in Figure 4. A figure of clean and used filters used in the TEOM system are pictured in Figure 5.

The TEOM system is equipped with a removable PM_{10} impactor inlet and a removable $PM_{2.5}$ cyclone. Sample air enters the TEOM system at a volumetric flow rate of 16.7 L/min, as this is the flow rate at which the impactor/cyclone are designed to operate. The flow is then split into two streams: a 3 L/min sample stream that goes to the TEOM filter housing and a 13.7 L/min bypass stream. The 3 L/min stream flows through the TEOM filter and deposits any entrained particulate matter on the filter. The two streams then recombine before being drawn through a

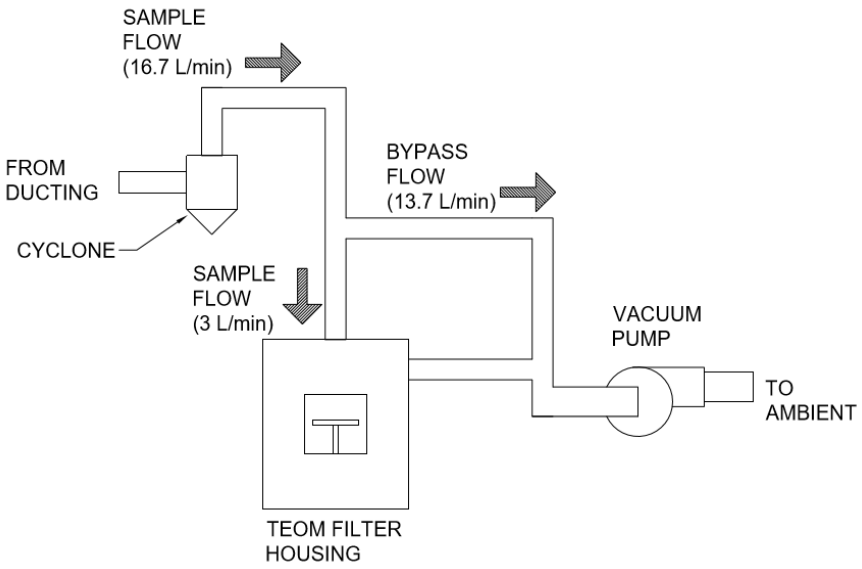

Figure 6: TEOM system flow path. The flow enters from the ducting at 16.7 L/min. It passes through the cyclone, and is then split into two flows: the bypass flow (13.7 L/min) and the sample flow (3 L/min). The sample flow passes through the TEOM filter housing, in which any entrained particulate mass is deposited on the filter. The sample flow then recombines with the bypass flow, which is then exhausted into ambient by a vacuum pump.

vacuum pump, which provides the motive force for the sampling. The flow is then exhausted into the laboratory after passing through a HEPA filter. The flow rates are controlled by two mass flow controllers which are internally calibrated for a standard environment of 25 °C and 101.3 kPa. The TEOM system flow path is shown in Figure 6.

The TEOM system's filter housing is kept at an elevated temperature of 50 °C. This is to eliminate any moisture condensing on the filter which would be sensed as additional mass. Past work has suggested that this elevated sample cell temperature drives off semi-volatile organic compounds as well, resulting in an underestimation of mass when compared to standard gravimetric methods in some circumstances (Green et al. 2009; Hauck et al. 2004; Cyrys et al. 2001). However, the

TEOM has also been shown to overestimate mass due to variations in particle mass median diameter (Wanjura et al. 2008), electrostatically charged particles (Meyer et al. 2008), and other reasons not fully understood (Vega et al. 2003; Edwards et al. 2006; Mohanjumar et al. 2011). The majority of comparison studies done between the TEOM and gravimetric methods have been done in ambient air sampling conditions over extended periods of time. The comparison done by Meyer et al. 2008 is the only known study that performs biomass combustion source sampling, which is similar to using the TEOM for cookstove applications. The wide range of correlations between the TEOM and gravimetric methods means a standard part of the TEOM protocol is a careful calibration against gravimetric test standards. Ad-hoc correction factors have been calculated by various groups, ranging from 0.6 (Mohankumar et al. 2011) to 1.3 (United Kingdom Department for Environment, Food, and Rural Affairs 2007).

There is also a correction factor internally programmed into the TEOM system, which is required for to bring the TEOM into agreement with gravimetric methods for EPA PM_{10} equivalency certification (EQPM-1090-079). The process to show equivalency to standard gravimetric methods for EPA certifications involves collocating three reference samplers (gravimetric) with three alternative samplers at a minimum of two separate sites (40 CFR 53.34). The correction factor used in the TEOM system is in the form of $y = 1.03x + 3$, where x is the raw mass concentration ($\mu m/m^3$) and y is the corrected mass concentration (ThermoFisher Scientific 2008). The coefficient values (1.03 and 3) are user-adjustable.

TEOM systems are designed to sample from the ambient environment at standard atmospheric pressure and to sample at particle concentrations much lower than those typically produced by cookstoves and captured by emissions hoods. For these reasons, using TEOM systems to quantify cookstove emissions monitoring requires significant modification.

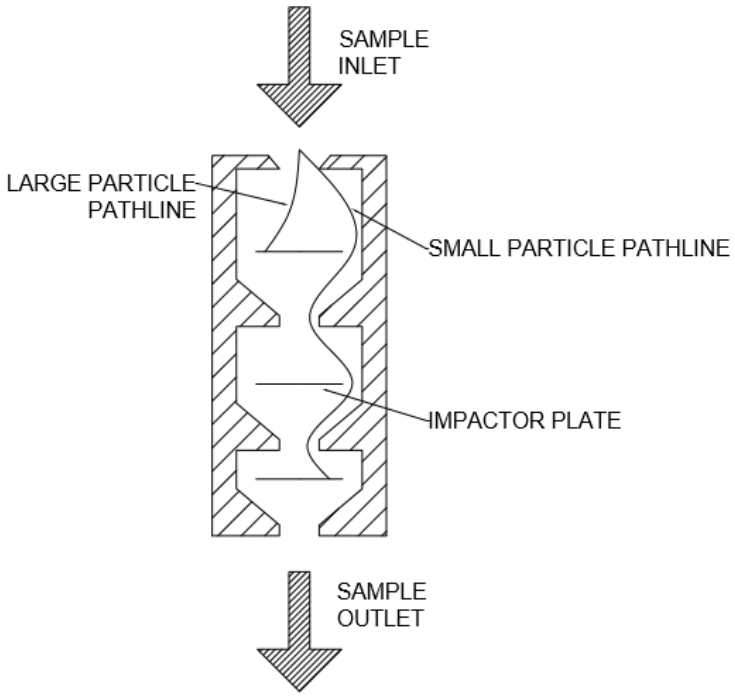

Figure 7: Three-stage cascade impactor operation. Each successive stage requires the particles to turn more sharply. Larger particles with larger inertias cannot follow streamlines at certain stages and are deposited on the impactor plates. In the example above, a large particle is immediately deposited on the first impactor plate, while a smaller particle is able to navigate through to the third stage where it is deposited.

1.6.4 Cascade Impactor

Cascade impactors are a well-known particulate matter sizing and analysis method. These impactors take advantage of particle inertia and aerodynamic drag. A cascade impactor is comprised of several stages in which the sample gas has to make a tight turn around an impactor plate. Larger particles do not follow the streamlines as closely as smaller particles, as the Stokes drag acting on the particles cannot overcome the larger particle inertias which results in the larger particles impacting the impactor plate. Each stage is designed such that only particles below a set cutoff aerodynamic diameter are allowed to pass, with everything larger being deposited on the impactor plates. The impactor plates are then weighed, which gives a binned distribution of

the particulate mass, as well as a total mass measure. A schematic of cascade impactor operation is shown in Figure 7.

As each impactor plate must be separately weighed before and after testing, cascade impactors are laborious to use. Cascade impactors are not typically used for cookstove analysis, primarily due to the labor intensiveness of the technique, and the size distribution of particulate matter from cookstoves is generally smaller than is optimal for impactor operation. They are, however, extensively used in aerosol inhalation studies and environmental monitoring.

1.6.5 Differential Mobility Analyzer

Differential mobility analyzers (DMA) are used to measure the size and number distribution of an aerosol sample. Several research groups have used differential mobility analyzers to characterize the size distributions of cookstove exhaust (Just et al. 2013; Jetter et al. 2012). Mobility analyzers work by first electrically charging particles in an aerosol sample. Larger particles become relatively highly charged due to their size, while small particles have relatively low charges. The charged particles are then passed through the ion inlet into the sample chamber, which is under an electric field. Once introduced into the sample chamber, the particles migrate according to the electric field strength and their charge. Larger particles migrate further than the smaller, less charged particles, and a particle size gradient is formed across the sample chamber. A carefully sized sheath of air is then drawn from the sample chamber. This sample contains a very small window of particle sizes, due to the particle size gradient. The number concentration is then measured using an aerosol particle counter. By varying the electric field in the sample chamber, the particle size gradient changes, and the sampled sheath air contains a different particle size range. A spectrum of particle sizes can then be measured and a size distribution can be constructed.

Modern differential mobility analyzers can scan through the particle size range of interest in as little as 16 seconds (SMPS Spectrometer 1936, TSI Inc., Shoreview, MN). This allows for quick

size distribution analysis without the manual work required for a cascade impactor, as well as allowing for a more continuous distribution (as opposed to discrete bins). However, differential mobility analyzers encounter many of the same particle characteristics dependencies as optical methods do. The shape, density, size, and chemical composition of the particles affect the charging rate, and particle diffusion, turbulence, and non-uniform electric fields can affect results (Alonso & Kousaka 1996; Santos et al. 2009). The design of the ion inlet can severely impact DMA resolution as well (Chen & Pui 1996) if the particles are not dispersed sufficiently.

1.7 Summary

Successful quantitative cookstove emissions and performance characterization is critically important in cookstove design and innovation to meet the WHO standards and ISO tiers. The ISO/IWA tier system is a method to allow straightforward comparison between stoves, and is based on WHO emissions rate goals. There are a range of testing methodologies used to compare and quantify cookstove performance. The most common are laboratory-based WBT comparison tests, due to their ease and simplicity. However, there is often a large disconnect between laboratory results and results seen in-field. There are a number of potential explanations for this discrepancy, namely different operating conditions in laboratory tests. Standardized tests also leave many testing decisions up to interpretation and the individual researcher, often leading to the "gaming" of these comparison tests to produce better performance results.

There is also a range of options for the cookstove testing suite used. Several testing suites have been described in the literature. Design decisions must be made as to the different analyzers required to fully characterize cookstoves, with cost, accuracy, and ease of use often being competing interests. As decreasing particulate matter emissions remains an elusive goal for cookstove designers, the choice of PM monitoring method is of particular importance. Current procedures used for PM analysis provide minimal information about cookstove performance, giving researchers an incomplete understanding of cookstove dynamics, highlighting the need for

time-resolved measurements of $PM_{2.5}$. Analyzer decisions are left to the individual laboratory, though the methodologies used should be fully reported in any comparison literature. The following section describes the laboratory testing suite designed and installed at the University of Washington.

Chapter 2: Cookstove Emissions and Performance Testing Suite

This chapter details the cookstove emissions and performance testing suite constructed at the University of Washington. Emphasis is placed on the hood and ducting construction as well as the gaseous emissions (CO_2 and CO) analyzers. Real-time quantitative particulate matter analysis is described in Chapter 3. The described system allows for quantitative performance and emissions testing of cookstoves to calculate the ISO cookstove comparison metrics. Uncertainty analysis is performed for each analyzer type (CO, mass, PM) in the context of the ISO tiers. A schematic of the cookstove emissions and performance testing suite is shown in Figure 8.

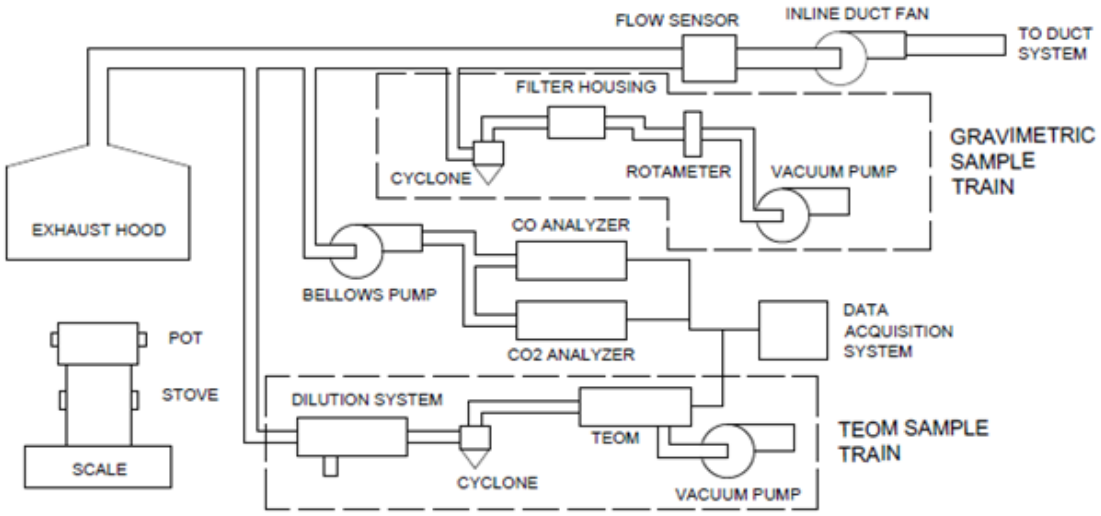

Figure 8: Cookstove emissions and performance testing suite. Stove emissions are captured by the hood and drawn through the ducting. Three sampling lines are installed: one for gas (CO/CO2) analysis and two for particulate matter analysis (gravimetric and TEOM). The remaining stove emissions are exhausted. The TEOM sample train is detailed in Chapter 3.

2.1 Hood and Ducting Design

In laboratory cookstove testing, the hood and ducting must be designed and calibrated properly, as the emissions comparison metrics are dependent on correct hood/ducting operation. The hood and ducting must collect all of the emissions from the cookstove so that the emissions metrics accurately describe cookstove operation and so that emissions do not escape into the surrounding laboratory, causing a potentially harmful environment for researchers. This must be balanced with a low enough flow rate as to not impact stove performance though inadvertent forced draft operation. The hood and duct must also be designed with the ranges of various analyzers in mind. As the additional air drawn by the hood dilutes the cookstoves emissions, the flow rate should be chosen to result in sufficient dilution so that the emissions concentrations are within normal operating ranges of the analyzers, yet large enough such that large uncertainties are not present. There are several considerations which must be taken into account during the design of the system.

2.1.1 Hood Design and Flow Rate

The emissions capture hood is constructed from 16 gauge sheet metal, enclosed on three sides with a support platform near the middle of the vertical support members to place the stove on. The hood then tapers near the top to accept 6” round ducting (6 in. 28-gauge galvanized round sheet metal pipe, Speedi-Products). The cookstove emissions are drawn up into the ducting which are then sampled by the CO/CO_2 and PM analyzers discussed in later chapters. Figure 9 shows the emissions hood installed at the University of Washington.

Figure 9: CAD model (left) and picture (right) of the hood and ducting emissions capture system. There are four rails which allow for the platform to be moved up and down. The platform is raised to the second highest rail setting. This gives a hood inlet face area of 40”x40” (WxH). The hood is 34” deep. The stove is placed on the platform during testing, with the emissions being captured and drawn into the ducting, which attaches from above. The flow through the emissions hood is drawn by a blower fan in the ducting.

There are four horizontal rails which allow the support platform to be moved up and down in 2” increments to change the face velocity of the hood, as well as the distance from the top of the stove to roof of the emissions hood. The main design considerations are the face area of the open side and the velocity of air entering the face (hood inlet face velocity). The area should be chosen such that the volumetric flow rate through the duct (determined by the choice of inline blower fan) entrains all of the cookstove emissions so that the resulting comparison metrics accurately describe the cookstove emissions performance. It is also important the no emissions escape the hood and enter the surrounding environment, causing a harmful environment for cookstove testers and researchers. However, the volumetric flow rate through the hood should not result in a significant hood inlet face velocity relative to the cookstove face velocity. This is

especially important when natural draft stoves are tested, as a hood inlet face velocity that is not significantly smaller than the cookstove face velocity may lead to inadvertent forced draft cookstove operation, affecting results.

The UW testing suite uses an inline duct fan (S-600, Vortex Powerfans, Terrebonne, Canada) set at 180 cfm (using a variable current limiter) to maintain constant flow in the ducting. The support shelf is placed at the highest position (40") with an open face area of 1,220 in^2. This results in a linear hood face velocity of 0.11 m/s. This is compared to a linear stove face velocity of a sample wood-fed natural daft cookstove of 0.53 m/s (calculated in Chapter 4.2). The stove face velocity is unique to each stove, though this provides a rough estimate for hood and ducting flow rate calibration. While there is not a recommended ratio of stove/hood face velocities, the hood face velocity should not excess 0.25 m/s (Aprovecho 2013) due to potential stove interactions.

The duct flow rate is monitored by a pitot type flow sensor (3100 Diamond Flow Sensor, Nailor, Houston, TX). The flow sensor outputs a differential pressure (ΔP), and is converted to a flow rate by using

$$Q = K * \sqrt{\Delta P} \qquad \text{Eq. 4}$$

Where Q is the flow rate in cfm, K is the K-factor calibration constant (supplied by the manufacturer) and ΔP is the differential pressure in inches of water. For the 6 in" ducting used, the K-factor is listed as 455. The differential pressure is converted into a voltage using a differential pressure transducer (Model 264, Setra, Boxborough, MA), which is then recorded by the data acquisition software (LabView, National Instruments, Austin, TX). The pressure is also displayed using a differential pressure gauge (Magnehelic 2000-00, Dwyer Instruments, Inc., Michigan City, IN).

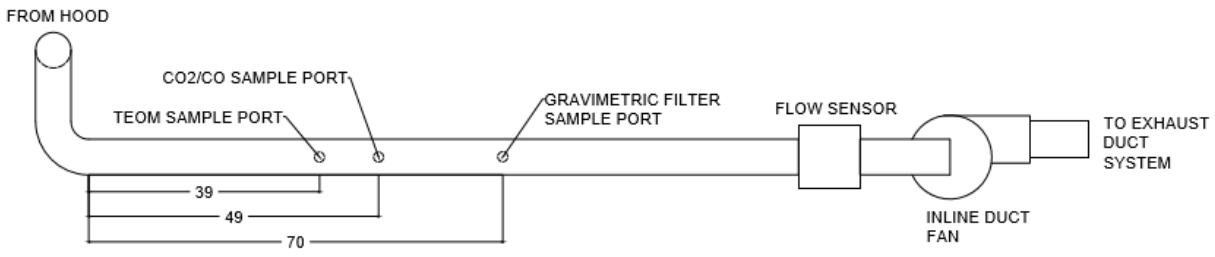

Figure 10: Ducting of cookstove comparison testing suite. Values are displayed in inches. The ducting extends 12" vertically from the hood cap before turning horizontal. Three sample ports (TEOM, CO/CO_2, and gravimetric filter) are installed in the straight section of ducting. Flow is drawn by an inline duct fan, and is exhausted into the facility's exhaust ducting system

To ensure that the flow sensor was reading accurately, a separate calibration procedure is used. Pure CO_2 is released directly into the ducting at the top of the emissions capture hood at a rate of 1.6 cfm. The CO_2 concentration further down the duct is then measured, and the required air to dilute the CO_2 to match the measured concentration is calculated using the following equations.

$$(\dot{m}_{CO2\ from\ tank} + \dot{m}_{Air} * y_{CO2\ in\ inlet\ air})/(\dot{m}_{Air} + \dot{m}_{CO2\ from\ tank}) = y_{CO2\ in\ duct} \qquad \text{Eq. 5}$$

$$(\dot{m}_{CO2\ from\ tank} - y_{CO2\ in\ duct} * \dot{m}_{CO2\ from\ tank})/(y_{CO2\ in\ duct} - y_{CO2\ in\ duct}) = \dot{m}_{Air} \qquad \text{Eq. 6}$$

where Equation 6 is rearranged from Equation 5. It was found that the difference between the two measures of flow rate (the flow sensor vs. the CO_2 calibration) is less than 3%.

Figure 11: Sample port in the ducting. The stainless steel tubing used is inserted 3" into the ducting, and flow is drawn through to the CO/CO_2 and gravimetric filter analyzers. CO_2 samplings were performed along the duct radius at sampling locations to ensure sufficient mixing has occurred. The samplings returned a uniform CO_2 profile, suggesting that the flow is homogenous in the ducting.

2.1.2 Ducting Design

The ducting is comprised of 6" round stainless duct members (6 in. 28-gauge galvanized round sheet metal pipe, Speedi-Products). An inline duct fan (S-600, Vortex Powerfans, Terrebonne, Canada) is installed near the end of the ducting to drive the flow through the hood and ducting system. A diagram of the ducting is shown in Figure 10.

Three ¼" stainless steel tube sample ports are located in the long straight ducting section. These sample ports allow for gas sampling for the TEOM, CO/CO_2, and gravimetric filter systems. The tubing is inserted 3" vertically into the ducting, perpendicular to the flow. Figure 11 shows a sampling port inserted into the ducting.

To ensure that sufficient mixing has occurred by the sample locations, pure CO_2 was injected into the hood and multiple CO_2 samplings were performed along the duct radius at the sample ports. These samplings returned a uniform CO_2 profile within the ducting system, suggesting the emissions from the cookstoves are well mixed at the sampling locations.

The uncertainty associated with a measure determined by a general function M with dependency on X and Y (with respective uncertainties of δX and δY) can be calculated as

$$\delta M = \sqrt{\left(\frac{\partial M}{\partial X} * \delta X\right)^2 + \left(\frac{\partial M}{\partial Y} * \delta Y\right)^2 + \cdots} \qquad \text{Eq. 7}$$

The measures of interest in the hood and duct system are the volumetric flow rate in liters per minute and moles per second. The volumetric flow rate in liters per minute is used for PM comparison metrics calculations, while the flow in moles per second is used in CO/CO_2 calculations. The flow rate is typically set at 5,097 L/min (180 cfm) or 3.48 mol/s. The flow rate in liters per minute is measured using an expanded version of Equation 1 with the required conversion, shown in Equation 8.

$$Q_{duct} = K * \sqrt{\Delta P} * C_{cfm \to L/min} \qquad \text{Eq. 8}$$

Where $C_{cfm \to L/min}$ is the conversion from cfm to L/min (28.3168). To convert the flow rate to moles/s, Equation 9 is used. The gases are assumed to be ideal.

$$\dot{n}_{duct} = Q_{duct} * \left(\frac{P_a}{R_{air} * T_a}\right) * \frac{1000}{60 * M_{air}} \qquad \text{Eq. 9}$$

Where P_a is the ambient pressure (Pa), R_{air} is the specific gas constant for air (J/kg/K), T_a is the ambient temperature (K), and M_{air} is the molar mass of air (g/mol). Table 3 lists the input variables with respective uncertainties. Using these values, the uncertainties of the hood and ducting system were calculated, resulting in uncertainties of the flow rates of ±40.5 L/min (0.8%) and ±0.03 mol/s (1.2%). The full uncertainty calculations are detailed in Appendix A.1.1.

Table 3: Uncertainties for hood and ducting variables

Variable	Nominal Value	Uncertainty	Notes
K	455	N/A	Given by manufacturer
ΔP	0.158" w.g.	±0.0025" w.g. (1% of full scale - set at 0.25" w.g.)	Uncertainty determined by pressure transducer.
T_a	21 °C	±0.1575 °C (±0.75% of reading)	

2.2 CO/CO_2 Analyzers

Both CO and CO_2 concentrations are continually monitored and recorded. Sample gas is drawn from the ducting using a bellows pump (MB-.158, Metal Bellows Inc., Sharon, MA) and filtered through a 12 micron inline fuel filter (FIL 3001, NAPA, Atlanta, GA). The flow rate is set at 5 SCFH using a rotameter. The flow is then split to each analyzer. CO concentrations are measured using a NDIR-type analyzer (VIA-510, Horiba, Kyoto, Japan). CO_2 concentrations are also measured using a NDIR-type analyzer (PIR-2000, Horiba, Kyoto, Japan). During cookstove testing, an initial 3 minute period is used to record the ambient levels of CO and CO_2. Gas concentrations recorded during the cookstove test are then normalized to account for background concentrations.

While CO_2 monitoring is not required by WBT protocols, we record CO_2 concentrations because it provides additional information on firing rate, and it can be used to estimate cookstove excess

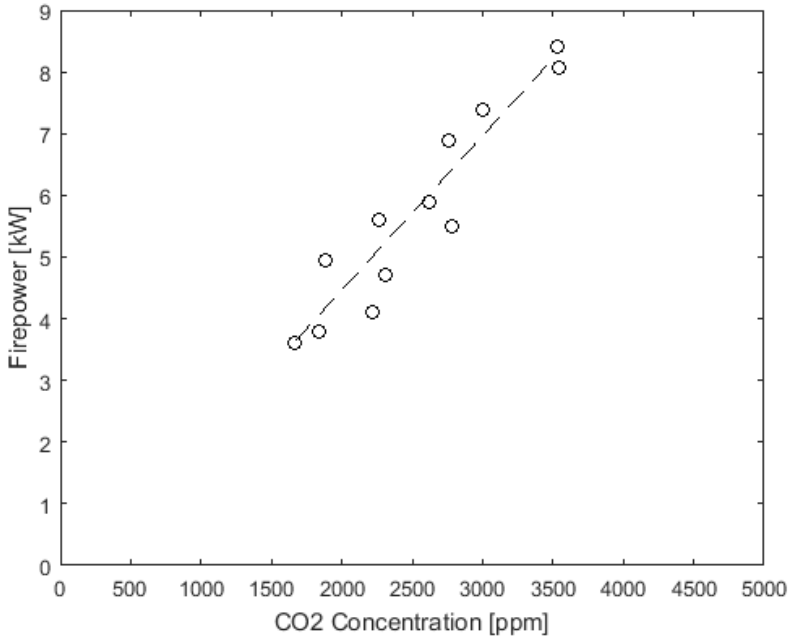

Figure 12: Firepower vs. CO_2 concentration measured in the ducting. A linear fit was calculated to be $FP = 2.5E-3 * y_{CO2} - 0.54$, where y_{CO2} is the measured CO_2 concentration and FP is the firepower of the stove. The R^2 of the fit is 0.88. This correlation allows the use of CO_2 concentrations as a proxy for cookstove firepower. This correlation is unique for each testing system, and should not be used across different testing suites.

air as discussed in Chapter 4. The CO_2 concentration can be a better indicator of firepower than instantaneous mass during a test, as it is difficult to disassociate the mass of evaporated water from the mass of wood consumed. Firepower is defined by the mass rate of consumed fuel multiplied by the fuel heating value. A correlation can be made by firing a stove with a covered pot and recording the instantaneous mass of the stove/pot/wood and CO_2 concentrations measured in the ducting. The firepower is then calculated from the decrease in mass measured by the real-time scale, and is plotted against the recorded CO_2 concentrations. A sample firepower correlation is shown in Figure 12. The correlation calculated ($FP = 2.5E-$

$3 * y_{CO2} - 0.54$ where y_{CO2} is the measured CO_2 concentration in the ducting and FP is the cookstove firepower) is only for the cookstove performance and emissions testing suite installed at the University of Washington. It is important that each testing center perform their own correlation, as the flow rate of the hood and ducting system will impact how much the cookstove emissions are diluted in the ducting. This correlation allows the measured CO_2 concentrations to be used as a proxy measurement for instantaneous firepower.

The uncertainty of the analyzer used is listed as ±1% of full scale (set at 2% CO_2 by volume), resulting in an uncertainty of 0.02% CO_2. Typical CO_2 concentrations measured in the ducting are near 0.25-0.30% CO_2. As the ISO tiers do not use CO_2 as a comparison metrics and all uses of CO_2 concentrations presented in this work are meant to be estimates, no further uncertainty analysis is performed regarding the CO_2 concentration measurements.

CO production is an ISO/IWA tiered metric, in both high and low power phases (g/MJ_d and g/min/L respectively). As the denominators of both metrics are dependent on weighed masses (with uncertainties covered in Chapter 2.3), the uncertainties given below only reflect the numerator uncertainty. The full ISO/IWA uncertainties are calculated in Chapter 5. The grams of CO produced is calculated using Equation 10.

$$g_{CO} = \sum_{t_0}^{t_{final}} y_{CO} * \dot{n}_{duct} * M_{CO} * \Delta t \qquad \text{Eq. 10}$$

Where y_{CO} is the measured concentration of CO (ppm), M_{CO} is the molar mass of CO (g/mo), $\dot{n}$ is the total molar flow rate in the duct (mol/s), and Δt is the length of time step (2 seconds), over which it is assumed the measured concentrations and flow rates remain constant. The grams of CO produced during each time step are then summed over the entirety of the test to give the total grams of CO produced. Table 4 lists the input variables with respective uncertainties. The

nominal value of the CO concentration is calculated assuming Tier 4 high power CO, 1.8 MJ_d, and 30 minute boil time, resulting in 14.5 g CO produced. The uncertainty is calculated for each time step and summed over the entirety of the test. This total summed uncertainty is calculated to be ±0.9 g (6.2%). The full uncertainty calculations are detailed in Appendix A.1.2.

Table 4: Uncertainties for CO variables

Variable	Nominal Value	Uncertainty	Notes
y_{CO}	165 ppm	±5 ppm (0.5% of full scale – set at 1,000 ppm)	
$\dot{n}_{duct}$	3.48 moles/s	±0.03 moles/s	Uncertainty calculated in Chapter 2.1.2
Δt	2 sec	0	

2.3 Mass Scale

The stove, fuel, and water mass are weighed using a digital scale (ABK 70a, Adam Equipment, Danbury, CT). The scale used has a 35 kg capacity and repeatability of ±1 g. The stove is placed on the scale for the duration of the test (with the pot of water on the stove). It is important that everything (stove, pot, water, and wood) is fully supported by the scale alone, so that there are no discrepancies with the measured mass. The scale is connected to the data acquisition software, enabling the recording of real-time mass measurement. This allows for the correlation of stove firepower and CO_2 concentration. During testing, CO_2 concentration can be a better proxy for firepower than the mass itself, as it is difficult to separate the contributions from burning wood verses evaporating water from the pot, both of which contribute to a decrease in overall mass. A lid on the pot eliminates complications due to water evaporation, but is not in compliance with the WBT protocol.

Mass readings are used for the calculation of several ISO/IWA tiered metrics, such as high power CO (g/MJ_d) and low power specific consumption (MJ/min/L). The megajoules delivered to the pot

(MJ_d) is calculated using Equation 11. The total megajoules produced is calculated using Equation 12a. Equation 12a uses the equivalent fuel consumed, which takes into account the moisture content in the wood and char produced during the test. The equivalent fuel consumed is calculated using Equation 12b.

$$MJ_d = \left(Cp_{water} * m_{water,0} * \left(T_{water,f} - T_{water,0}\right)\right) + \left(\Delta H_{vap,water} * \left(m_{water,0} - m_{water,f}\right)\right) \quad \text{Eq. 11}$$

$$MJ = m_{wood,eqv.} * HV_{wood} \quad \text{Eq. 12a}$$

$$m_{wood,eqv.} = \frac{m_{wood} * \left(HV_{wood} * (1 - mc) - \left(mc * Cp_{water} * \left(T_{water,f} - T_a\right) + \Delta H_{vap,water}\right)\right) - m_{char} * HV_{char}}{HV_{wood}} \quad \text{Eq. 12b}$$

Where Cp_{water} is the specific heat of water (J/g/°C), m_{water} is the mass of the water (kg), T_{water} is the temperature of the water (°C), $\Delta H_{vap,water}$ is the latent heat of vaporization of water (J/g), T_a is the ambient temperature (°C), $m_{wood,eqv.}$ is the equivalent mass of fuel consumed (g), HV is the heating value of the wood and char (kJ/kg), m_{wood} is the measured mass of fuel consumed (g), mc is the percent moisture content of the wood, and m_{char} is the mass of char produced (g). Subscripts 0 and f denote measurements taken at the start and end of the test, respectively.

It is important that the wood used is homogenous across comparison tests, as several factors can impact the heating value of the wood. The carbon content in wood varies depends on where in the tree the wood was harvested from as well as its mass fractions of earlywood (formed in the spring) season and latewood (formed in the winter season) (Lamlom & Savidge 2003). As it's impractical to measure the heating value of all of the wood used, it is important to use uniform wood supplies so that comparisons can be successfully made across tests. Table 5 lists the input variables for mass calculations with respective uncertainties. Nominal values for MJ_d and MJ for high power thermal efficiency are 1.8 MJ and 4 MJ, respectively. These values are dependent

on stove operation and represent a stove with 45% thermal efficiency (Tier 4). Calculated uncertainties for MJ_d and MJ are ±0.01 MJ_d (0.6%) and ±0.04 MJ (1.0%). The full uncertainty calculations are detailed in Appendix A.1.3.

Table 5: Uncertainties for Mass Variables

Variable	Nominal Value	Uncertainty	Notes
$m_{water,0}$	5,000 g	±1 g	
$m_{water,f}$	4,940 g	±1 g	Nominal value comes from a real test.
m_{wood}	240 g	±1 g	Nominal value comes from a real test
m_{char}	5 g	±1 g	Nominal value comes from a real test
$m_{wood,eqv.}$	208 g	±2.5 g	Uncertainty calculated (Appendix A.1.3)
$T_{water,f}$	95 °C	±0.7125 °C (±0.75% of reading)	
$T_{water,0}$	15 °C	±0.1125 °C (±0.75% of reading)	
T_a	21 °C	±0.1575 °C (±0.75% of reading)	
HV_{wood}	19,314kJ/kg	0	Commonly used value (Global Alliance for Clean Cookstoves 2014b)
HV_{char}	29,500 kJ/kg	0	Commonly used value (Global Alliance for Clean Cookstoves 2014b)
mc	0.09	±0.005	

Chapter 3: Time-resolved PM2.5 Measurement of Wood-Fed Natural Draft Cookstoves using a Tapered Element Oscillating Microbalance

This chapter details the setup, operation, and necessary calibration of the tapered element oscillating microbalance system (TEOM) for cookstove particulate matter analysis. Several changes to the system (internal and external) are required for cookstove application, such as the addition of an external dilution system. Select results are also presented using this system, showing that the TEOM provides additional information that otherwise would not be available to researchers using current particulate matter analysis methodologies, such as the measurement of transient high PM events during cookstove refueling as well as time-resolved PM production during start-up.

3.1 Required Changes to the TEOM system

Tapered element oscillating microbalance systems have not been used for cookstove particulate matter analysis. Described more fully in Chapter 2.4.3, the TEOM system allows for time-resolved direct particulate matter mass measurement. Because the system was originally designed for long-term ambient air monitoring, several changes were required for successful application.

Many of the internal controls of the TEOM are designed for long-term ambient air monitoring, in which metrics of interest are 12 and 24 hour concentration averages. The TEOM is originally programmed with a 300 second rolling averaging function. This eliminates the majority of noise and transient events, though transient events are of particular interest in cookstove analysis. The rolling average time was adjusted to 10 seconds. This gives finer time resolution and allows for transient PM events to be recorded. This does result in an increased level of noise, though this noise does not have a significant effect on the total mass measured.

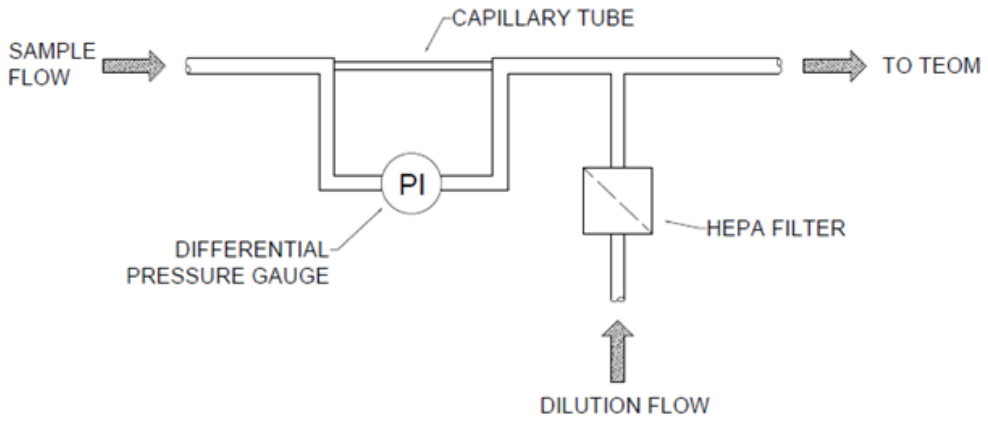

Figure 13: External particulate matter dilution system. The sample flow is restricted by the capillary tube, with the balance of the flow made up by the HEPA filtered dilution flow. The flow rate of the sample flow is determined by measuring the pressure drop across a capillary tube. Dilution ratio can be changed by altering the diameter or the length of the capillary tube, as well as by adding length of tubing to the diluent stream, all of which modify the flow resistances and the respective flows

As mentioned above, the TEOM system is also originally programmed with an internal correction factor in the form of $y = 1.03x + 3$, where x is the raw mass concentration (µm/m^3) and y is the corrected mass concentration (ThermoFisher Scientific 2008). This correction is required for the TEOM system to align standard gravimetric filter methods for EPA PM_{10}. The correction factor coefficients (1.03 and 3) are user-adjustable, though they were kept at their default settings for this work.

3.1.2 TEOM External Dilution System

For particulate emissions monitoring from cookstoves, the TEOM requires an additional dilution system because the PM loading directly from the ducting would necessitate frequent filter changes (a filter change would need to be performed after every test). The TEOM external dilution system is shown in Figure 13 and Figure 14.

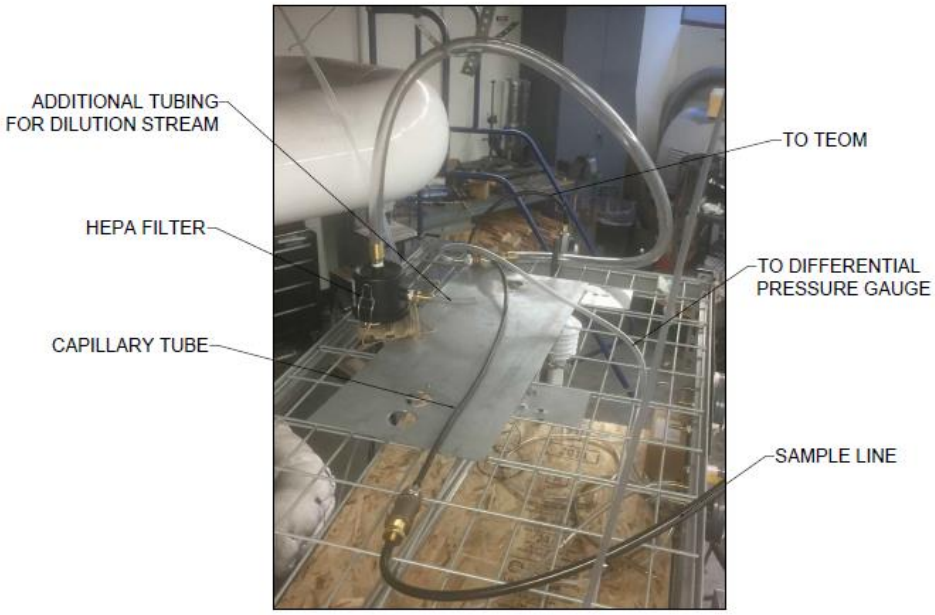

Figure 14: External dilution system required for TEOM cookstove application. The capillary tube and the additional tubing for dilution stream lengths can be changed to modify the resulting dilution ratio. The flow rate through the capillary tube (sample flow) is measured by monitoring the pressure drop across the tubing. All tubing is anti-static.

The dilution system is based on widely used commercial systems that dilute the flow using capillary tubes (or some other flow restrictions) in the sample stream and a separate stream, open to the environment, makes up the balance of the flow with filtered air, both drawn by a backside pump. The dilution system limits and measures the flow rate from the sample stream (from the hood ducting) and then provides HEPA (CSL-825-039HCB, Solberg Mfg., Itasca, IL) filtered make-up air through a parallel channel. These two streams are drawn by a separate vacuum pump (packaged with the TEOM system) that draws a flow rate controlled by two internal (to the TEOM) mass flow controllers. The dilution system consists of a 27” long, 3/8” outer diameter static-dissipative black silicone rubber sample capillary tube (1909T7, McMaster-Carr, Santa Fe Springs, CA). The sampling flow rate through the capillary was characterized using a bubble flowmeter (Gilibrator-2, Sensidyne, St.Pertersburg, FL), with the differential pressure across the

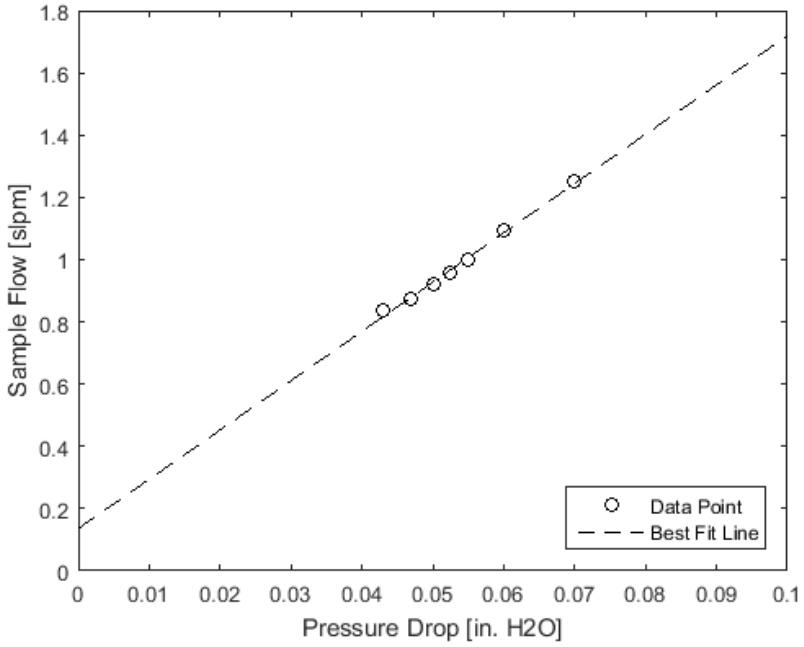

Figure 15: Volumetric flow rate through the sample capillary tube vs. pressure drop across the tube. The best fit line was calculated to be $Q_{sample} = 15.84 * \Delta P_{capillary} + 0.14$, with an R^2 value of 0.9932.

capillary monitored with a differential pressure gauge (Magnehelic 2000-00N, Dwyer Instruments, Inc., Michigan City, IN). The flowrate and pressure drop relationship of the dilution capillary tube is shown in Figure 15. A linear fit resulted in the line equation of $Q_{sample} = 15.84 * \Delta P_{capillary} + 0.14$, where $\Delta P_{capillary}$ is the measured pressure drop across the capillary tube (in. H_2O), and Q_{sample} is the sample volumetric flow rate (L/min). The fit has an R^2 value of 0.9932.

The dilution system is made up of compression fittings and 3/8" static-dissipative silicone rubber tubing and is connected directly to the TEOM system's cyclone. The TEOM uses a 16.7 L/min, 2.5 µm cutoff cyclone (BGI Sharp Cut Cyclone, Mesa Labs, Inc., Butler, NJ). The length of the capillary tube controls the desired dilution through its intrinsic flow resistance. Additional tubing can also be added to the HEPA filter stream to increase its resistance, decreasing the dilution ratio. The dilution rate is calculated by $DL = Q_{sample}/(Q_{sample} + Q_{dilution})$, where the subscripts

sample and *dilution* denote the flow rate through the sample line (from the exhaust ducting) and the flow rate through the dilution line, respectively. We use a dilution rate of 1/18.75 because it results in high enough PM concentrations to minimize measurement uncertainty, while avoiding frequent filter changes. At our current dilution ratio, the TEOM filter requires changing roughly every 30 tests, compared to changing filters after every test without the external dilution system. The dynamic range of the TEOM system is 0-5,000,000 $\mu g/m^3$. Typical PM concentrations experienced from cookstove emissions while using the external dilution system are 0-3,000 $\mu g/m^3$, while the national standard for annual ambient $PM_{2.5}$ (the original design purpose of the TEOM system) is 12 $\mu g/m^3$ (United States Environmental Protection Agency 2012). We conducted flow audits bimonthly to ensure minimal flow rate drift in the dilution system and found that the system drifted less than 5%.

3.1.2.1 Particle Penetration Calculations

Particle penetration efficiency (defined as the percent of particles that reach the TEOM from the hood ducting) was calculated to be greater than 99% for particles 2.5 µm in diameter and 98.3% for particles 0.1 µm in diameter. Smaller particles experience larger diffusional losses than particles with a larger diameter. There were initial concerns that particles may be lost due to the additional dilution system tubing. Several loss mechanisms are considered, namely diffusion and inertial deposition due to enlargements/contractions in the dilution system. Once the dilution and sample flow combine immediately before entering the TEOM system, the flow becomes transitional (Re = 3,700) and turbulent inertial deposition is also taken into account. The individual penetration efficiencies are then multiplied together to give a total penetration efficiency for the entire dilution system, which is calculated to be 98.3%. The following Table 6, Table 7, and Table 8 detail these particle penetration efficiency calculations for particles 0.1 µm in diameter.

Table 6: Particulate matter characteristics

Variable		Units
Particle Density	600 (Rockne et al. 2000)	kg/m^3
Particle Diameter	0.1	µm

Table 7: Dilution system component penetration efficiencies

Item	Occurrences	Equation	Resulting Penetration Efficiency
Sampling Probe	1	Eq. 13a	0.9984
Anti-Static Tubing A	1	Eq. 13a	0.9931
Enlargement	2	N/A	1
Tee	2	Eq. 13a	0.9990
Contraction	2	Eq. 14a	0.9943
Capillary Tube	1	Eq. 13a	0.9999
Anti-Static Tubing B	1	Eq. 13a and 15a	0.9995
Total Penetration Efficiency			0.9833

Table 8: Dilution system component characteristics

Item	Length [m]	Diameter of inlet [m]	Diameter of outlet [m]	Q [L/min]	Velocity [m/s]
Sampling Probe	0.1016	0.004572	0.004572	0.85	0.853
Anti-Static Tubing A	0.9271	0.00635	0.00635	0.85	0.442
Enlargement	N/A	0.00635	0.0127	0.85	0.442
Tee	0.0508	0.0127	0.0127	0.85	0.111
Contraction	N/A	0.0127	0.00635	0.85	0.111
Capillary Tube	0.6985	0.00635	0.00635	0.85	0.442
Enlargement	N/A	0.00635	0.0127	0.85	0.442
Tee	0.0508	0.0127	0.0127	0.85	0.111
Contraction	N/A	0.0127	0.00635	16.7	2.197
Anti-Static Tubing B	0.38735	0.00635	0.00635	16.7	8.789

$$\eta_{diff} = 1 - 5.50\mu^{\frac{2}{3}} + 3.77\mu$$ Eq. 13a (Hinds 1982)

$$\mu = \frac{DL}{Q}$$ Eq. 13b (Hinds 1982)

Where η_{diff} is the penetration efficiency due to diffusional losses, D is the particle diffusion coefficient, L is the component length, and Q is the volumetric flow rate through the component. Equation 10 is used to calculate particle losses in the tubing due to diffusion.

$$\eta_{inert} = \left[1 - e^{1.721 - 8.557x + 2.227x^2}\right]^2$$ Eq. 14a (Willeke & Baron 1993)

$$x = \frac{\sqrt{Stk}}{\left(\frac{D_i}{D_n}\right)^{0.31}}$$ Eq. 14b (Willeke & Baron 1993)

Where η_{inert} is the penetration efficiency due to inertial losses, D_i is the diameter of the inlet and D_n is the diameter of the outlet nozzle. Equation 11 is used to calculate particle losses due to enlargements and contractions in the tubing.

$$\eta_{turb\ inert} = e^{-\frac{\pi L V_t}{Q}}$$ Eq. 15a (Weiden et al. 2009)

$$V_t = \frac{\left(6 * 10^{-4}\left(0.0395\ Stk\ Re^{\frac{3}{4}}\right)^2 + 2 * 10^{-8}\ Re\right) * U}{5.03\ Re^{\frac{1}{8}}}$$ Eq. 15b (Weiden et al. 2009)

Where $\eta_{turb\ inert}$ is the penetration efficiency due to turbulent inertial losses, L is the component length, Q is the volumetric flow rate through the component, and V_t is the turbulent inertial deposition velocity. Equation 15 is used to calculate particle losses due to turbulent inertial losses.

3.1.3 TEOM Pressure Sensitivity

We found that the TEOM system PM output was sensitive to pressure changes at the TEOM inlet due to the reliance on internal mass flow controllers. The volumetric flow rate through the TEOM must be manually corrected using local pressure to keep the flow rate within acceptable limits. The local pressure can be programmed into the TEOM using the front interface screen. The TEOM system is also sensitive to temperature changes, though an externally mounted temperature/humidity sensor automatically corrects for the local temperature. We monitored the input pressure into the TEOM by measuring the differential pressure between the hood ducting dynamic pressure and atmospheric pressure as well as the pressure drop across the capillary tube using a differential pressure gauge, and ensured that this corrected pressure is manually programed in the TEOM system weekly. The corrected pressure is calculated by $P_{actual} = P_{atm} - \Delta P_{sys}$, where ΔP_{sys} is the differential pressure between the TEOM inlet and ambient pressure. ΔP_{sys} is calculated by $\Delta P_{sys} = \Delta P_{duct} + \Delta P_{capillary}$, where ΔP_{duct} is the differential pressure between the ducting and ambient pressure, and $\Delta P_{capillary}$ is the differential pressure across the capillary tube in the dilution system. P_{actual} can also be calculated by measuring the differential pressure between the inlet of the TEOM and ambient pressure directly, though ΔP_{duct} and $\Delta P_{capillary}$ are already measured for ducting and dilution system flow rate calculations, respectively and are used out of convenience.

3.2 Calibrating the TEOM to Standard Gravimetric Method

We compare measurements of $PM_{2.5}$ between the standard gravimetric filter method and the TEOM for standard and abbreviated water boil tests, as the gravimetric method is considered the best calibration standard. This comparison is used to determine a calibration correction for the TEOM to report values consistent with the gravimetric method.

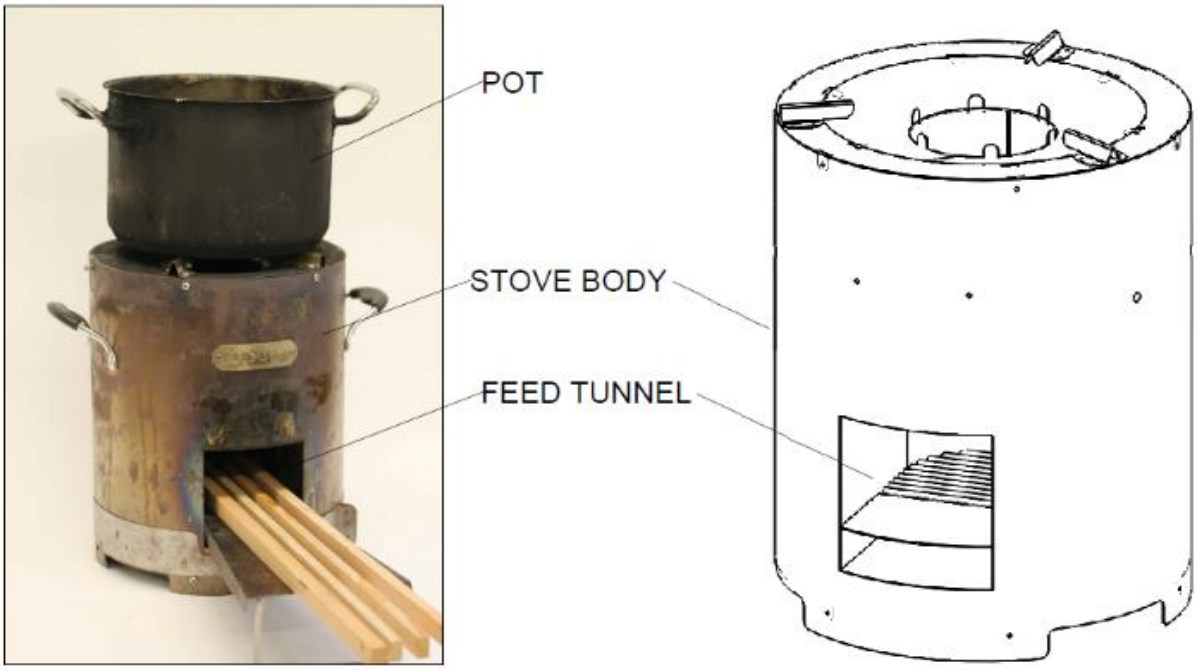

Figure 16: Burn Design Lab cookstove used for the TEOM vs. gravimetric comparison. The body is 28 cm in diameter and 36 cm tall. An 11 cm diameter vertical riser extends from the top of the feed tunnel, concentric with the stove body.

3.2.1 Experimental Setup and Results for TEOM vs. Gravimetric Comparison

The gravimetric filter sampling train consists of a 16.7 L/min, 2.5μm cutoff Teflon coated aluminum cyclone (URG-2000-30EH, URG Corp., Chapel Hill, HC) and a filter housing for 102mm diameter borosilicate glass micro-fiber filters (FPAE-102, Hi-Q Environmental Products Company Inc., San Diego, CA). Downstream of the filter there is a rotameter calibrated for 16.7 L/min flow rate during operation (calibrated using an inline wet test meter upstream of the rotameter) and a vacuum pump (RTD874A, Gast Mfg., Benton Harbor, MI). The components of the gravimetric filter sampling train are connected with 5/8" high-pressure clear Tygon PVC tubing, with the sample being exhausted after passing through the pump. The filters are desiccated at room temperature for 24 hours and weighed three times (AE163, Mettler Toledo, Columbus, OH). We install a filter into the housing, turn on the vacuum pump, and record the time. Then the stove is lit using

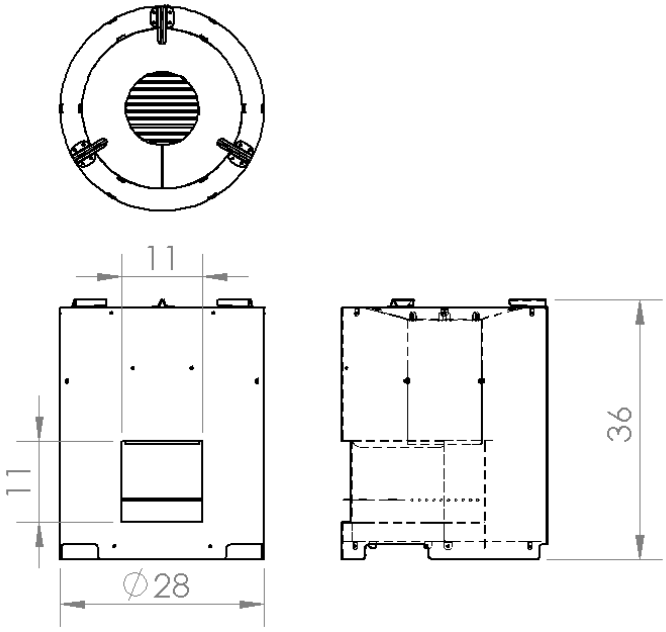

Figure 17: Dimensioned drawing of BURN Design Lab prototype cookstove.

kindling and paper towels and operated under WBT guidelines. Once a sufficient mass is accumulated (determined by the TEOM total mass read-out), the stove is extinguished and the vacuum pump is turned off, again with the time recorded. The filter is removed and desiccated again for 24 hours before being weighed three times to establish the particulate mass deposited. The recorded time stamps are used to determine the differential mass the TEOM records. This procedure is repeated for various total masses by varying burn length and rate. The total $PM_{2.5}$ mass produced by the stove is calculated as $\Delta M = \Delta M_{meas} \cdot Q_{duct}/Q_{sys}$, where ΔM_{meas} is the mass measured by the gravimetric method or TEOM, Q is the flow rate, and the subscripts *sys* and *duct* denote the flow rate required by the system (3 L/min for the TEOM and 16.7 L/min for the gravimetric filter) and the flow rate through the ducting, respectively.

We use a Burn Design Lab (Vashon, WA) prototype natural draft wood-fed rocket cookstove. The stove is made from 0.6 mm thick sheet metal with a 0.8 mm thick stainless steel combustion

chamber. The combustion chamber is wrapped in 1" fiberglass insulation. A feed tray (pictured underneath the wood) is used as a platform to support the wood as it is fed through the feed tunnel into the combustion chamber. An image and schematic of the cookstove is shown in Figure 16 and Figure 17.

The unprocessed TEOM readout is found to not quantitatively agree with the gravimetric measurements. For this reason we ran a series of experiments in an effort to clarify the discrepancy. The objective was to determine if there was any inconsistency in TEOM or gravimetric operation that may explain the difference between the two methods. A series of hypotheses were developed, and six modifications of the sampling train and TEOM operating conditions were examined. A list and descriptions of these modifications are provided in Table 9. Previous long-term ambient air studies have shown that sample cell temperature plays an important role in mass (and mass concentration) discrepancies (Green et al. 2009), with the vaporization of semi-volatile organic compounds being a major cause (Mignacca & Stubbs 1999). For this reason, we conducted measurements at the factory default cell temperature of 50 ºC as well as the lowest allowed setting of 30 ºC. There was also concern over the fact that the two cyclones, one for the TEOM and the other for the filter, have slightly differing penetration efficiencies. The cyclones for both sampling trains were removed to test their effect. To investigate the role of water vapor produced from the combustion process and evaporation from the boiling water, tests were run without desiccating the gravimetric filters post-test, with the hypothesis being that the TEOM system records a portion of this water vapor as particulate mass**.** We also interchanged the duct sample ports to test whether duct non-uniformity caused any bias between the two methods. In the original configuration, the TEOM sample point is upstream of that for the gravimetric system. The modified configuration has the gravimetric system sampling upstream of the TEOM system. The gravimetric cyclone claims to operate identically in both vertical and horizontal arrangements, however we hypothesized that some particulate matter was

being lost (falling off) during the transfer from the filter housing to the Petri dish before being desiccated. We tested the cyclone in both horizontal and vertical arrangements.

Table 9: Modifications performed to compare the TEOM and gravimetric filter methods.

Modification	Description	Number of Expts.
50 Degrees	Default TEOM settings with sample cell at 50 ºC	42
30 Degrees	Sample cell set to 30 ºC	22
Removed Cyclones	Both cyclones were removed	11
No Desiccation	Gravimetric filters not desiccated before post-test weighing.	18
Switched Sample Ports	Sampling locations were switched	24
Vertical Cyclone	Gravimetric cyclone mounted vertically	16

We conducted 133 experiments under various modifications and PM loading, comparing the standard gravimetric filter method and the TEOM system. Figure 18 shows a plot of the total PM mass measured by the TEOM system versus the total PM mass collected by the gravimetric system for the variety of modifications described in Table 9. This figure shows that there is a linear relation between the TEOM and gravimetric measured total mass, however, the TEOM consistently reports higher total mass. In addition, it is not readily apparent if any of the modifications applied (Table 9) result in significant difference in the TEOM measured mass. We perform a variety of statistical analyses in an effort to interpret the different treatments and to provide a single calibration correction for TEOM results relative to the gold standard gravimetric method.

There are many potential sources of error when dealing with small differential masses (median ΔM_{Grav} is 0.833 mg) so we employ robust regression with Tukey bisquare weighting (k = 4.685) to establish potential linear models (Fox 2002). A Tukey bisquare model weights outliers less than traditional least squares regression models, resulting in a line fit that is not as significantly impacted by outliers that may be caused by weighing errors. The first model considered was a single linear fit “lumped” model, with all of the data considered to be part of the same data set.

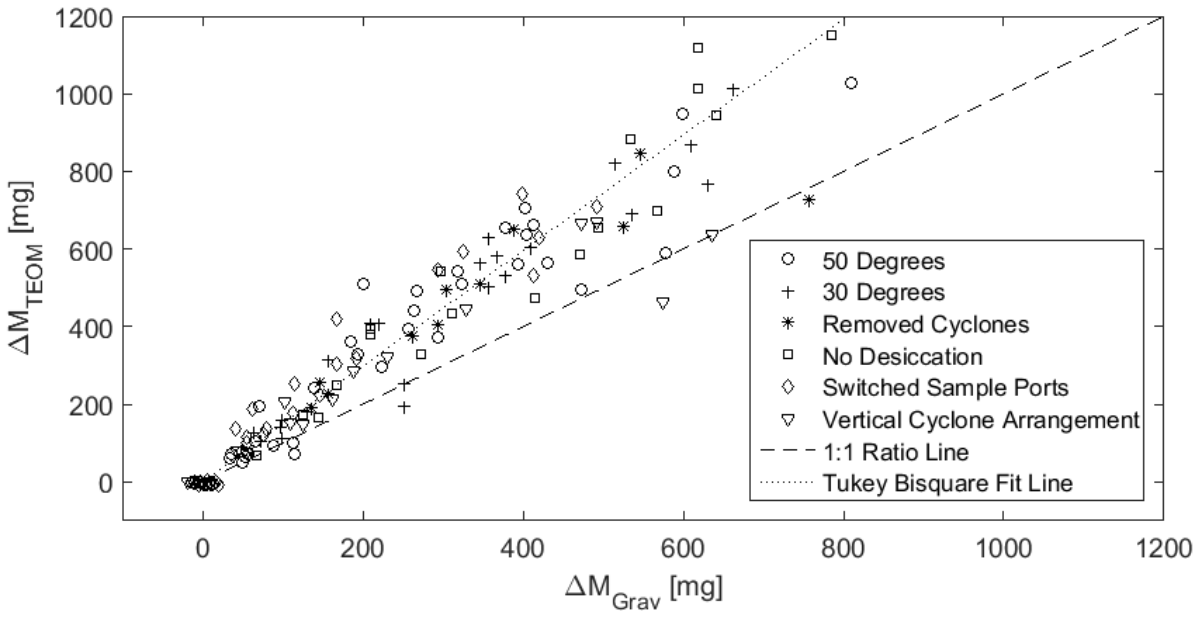

Figure 18: Plot of the mass collected by the TEOM ΔM_{TEOM} versus the mass collected by the gravimetric system ΔM_{Grav} produced for various modifications. The TEOM consistently reports higher total mass compared to the gravimetric filter. The dashed line shows the 1:1 ratio line (complete agreement of the data) and the dotted line shows the best fit line (using Tukey Bisquare robust regression) of the data, found to be y = 1.49x.

The second model treated each modification separately with its own linear fit. We performed Akaike Information Criterion (AIC_C) analysis (Posada & Buckley 2004) to determine which model (lumped vs. unlumped) is more likely to be representative of the data. The AIC_C is defined as $AIC_c = N \ln\left(\frac{SS}{N}\right) + 2K + \frac{2K(K+1)}{N-K-1}$, where *K* is the number of parameters fit plus one, *SS* is the weighted sum of squares, and *N* is the number of data points (Posada & Buckley 2004). The results of the AIC_C analysis are shown in Table 10. The lumped model is found to be the more likely model, with an evidence ratio of 6,634.

Table 10: Results of AIC_C analysis for lumped vs. unlumped models

Model	Sum of Squares	N	Parameters	$AIC_{C`}$	Probability	Evidence Ratio
Lumped	3.8769e+05	133	2	1.0651e+03	99.99%	6,634
Unlumped	3.7358e+05	133	12	1.0827e+03	0.01%	

A second analysis was then performed to determine whether a lumped model in the form of $y = Ax+b$ or $y = Ax$ is more likely to be the correct model. The results are shown in Table 11.

Table 11: Results of AIC_C analysis for lumped models in the form of y = Ax+b vs. y = Ax

Model	Sum of Squares	N	Parameters	$AIC_{C`}$	Probability	Evidence Ratio
Lumped $y = Ax+b$	3.8769e+05	133	2	1.0651e+03	0.01%	19,930
Lumped $y=Ax$	3.3925e+05	133	1	1.0453e+03	99.99%	

The analysis resulted in an evidence ratio of 19,930, in favor of the lumped model in the form of $y = Ax$. The best fit line of the model selected by AIC_c analysis is $y = 1.49(\pm0.05)x$ and is plotted in Figure 18. Using this fit, a calibration factor of 1/1.49 was then applied to the TEOM total mass produced data to force it along the 1:1 ratio line. The corrected results are shown in Figure 19. The WBT high-power PM tier locations were calculated assuming 1.8 MJ, the average in our tests, delivered to the pot. After correction, the best fit line equation is $y = 1.00(\pm0.03)x$**.** The use of calibration factors for the TEOM system is an accepted practice. As mentioned before, the TEOM is internally programmed with a correction factor in the form of $y = 1.03x+3.00$ where x is the uncorrected mass concentration ($\mu m/m^3$), and y is the corrected mass concentration. This correction factor was necessary for the TEOM to receive EPA PM_{10} equivalency certification. Other work has suggested correction factors ranging from 0.6 (Mohankumar et al. 2011) to 1.3 (United Kingdom Department for Environment, Food, and Rural Affairs 2007). While these groups have suggested several mechanistic explanations for the discrepancies they have described, we

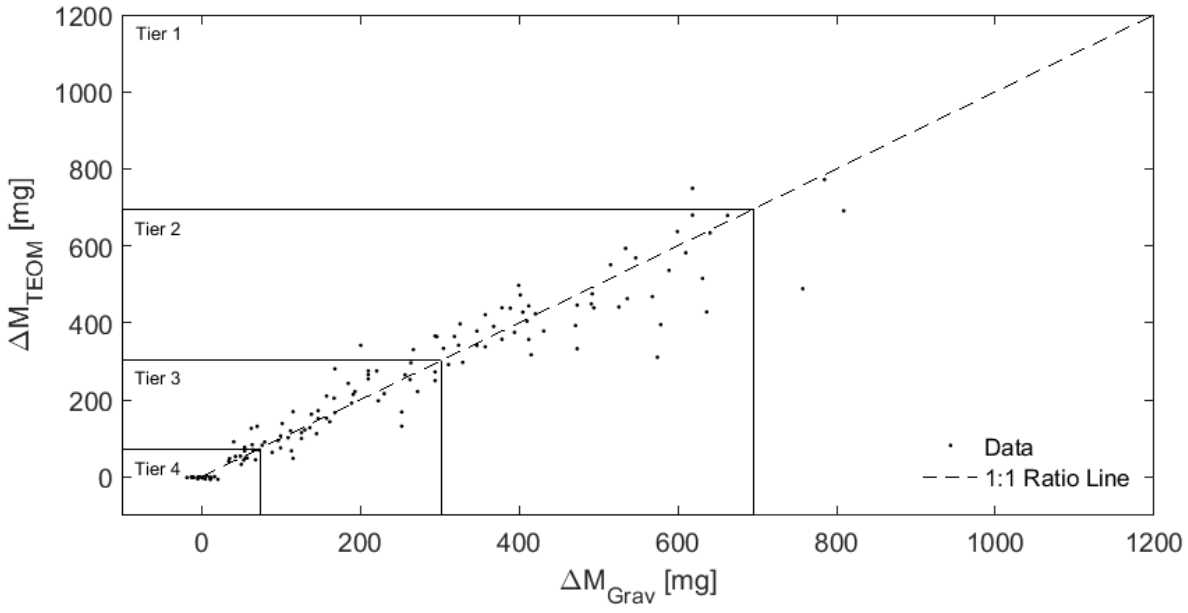

Figure 19: Corrected ΔM_{TEOM} vs. ΔM_{Grav} filter comparison, with WBT high-power PM tiers. A correction factor of 1/1.49 is applied to the TEOM data to make it fall on the 1:1 ratio line (shown as the dashed line). Also shown are the ISO/IWA 11:2012 high-power PM tier locations, assuming 1.8 MJ delivered to the pot. This shows that the correlation holds over the range of interest to cookstove developers.

do not fully understand the cause of the discrepancy that appears in our work. It may be a combination of several compounding factors, though more work needs to be completed to definitively ascertain the cause of the discrepancy between the TEOM and the standard gravimetric filter method.

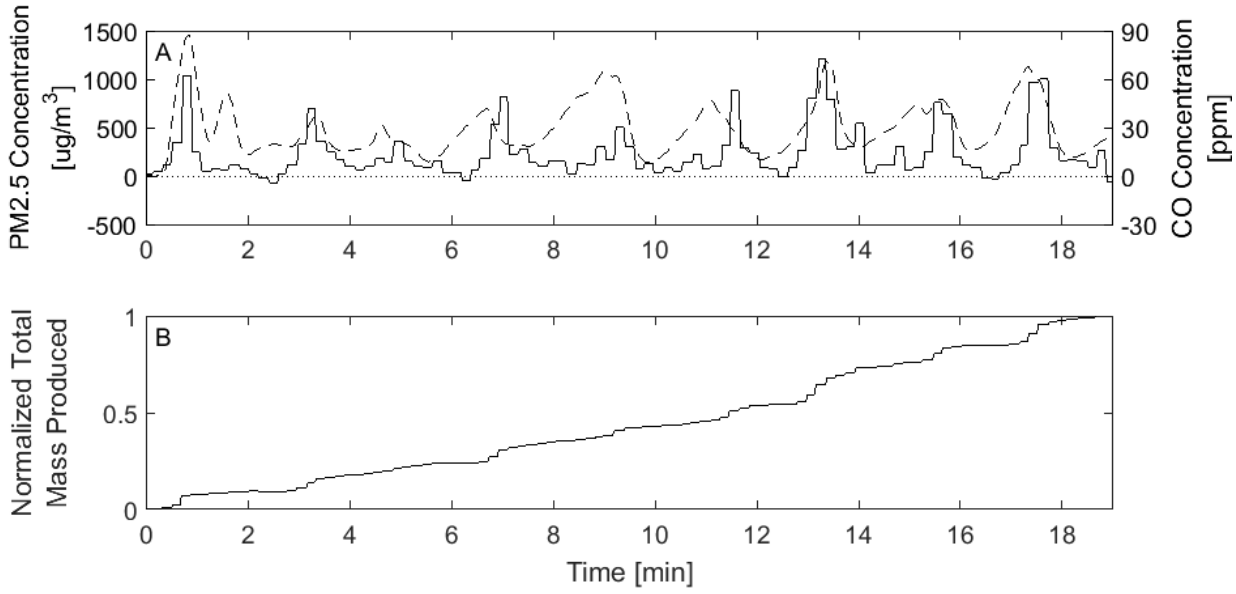

Figure 20: Correlation of TEOM $PM_{2.5}$ (solid) and CO (dashed) over time during an abbreviated WBT and normalized cumulative total particulate mass produced of a baseline cookstove. There is a strong correlation between the PM and CO because both $PM_{2.5}$ and CO are produced by incomplete combustion. The spike in CO/PM at one minute and every following two minutes is caused by loading new cold fuel into the combustion chamber. This refueling is accompanied by a large spike in $PM_{2.5}$ concentration. These spikes contributed significantly to the overall particulate matter production, with roughly 37% of the particulate mass being produced during refueling events in this test.

3.4 Application of TEOM to Time-Resolved $PM_{2.5}$ Measurement to Stove Evaluation and Design

Time-resolved $PM_{2.5}$ data provide researchers quantitative $PM_{2.5}$ over the course of a burn. This enables the correlation of sooting events with physical actions or operational variations. It also enables rapid progression from the high power boil phase to the simmer phase during WBTs which result in more precise measurements, as the time needed to change filters for standard gravimetric methods can result in skewed mass measurements due to additional evaporated water during the weighing. Figure 20a shows a plot of TEOM $PM_{2.5}$ and carbon monoxide

concentration as a function of time. The data shows that the PM and CO are strongly correlated. The peaks that occur at one minute and every two minutes (~3, 5, 7 minutes) correspond to events where fuel is added into the combustion chamber by the operator, usually breaking off some amount of char in the process. A total of 372.63 mg $PM_{2.5}$ was produced during this specific test with roughly 37% of the mass being produced during refueling events. We believe that these spikes are the result of unburnt low-temperature wood being volatized quickly after introduction into the combustion chamber, during which time the wood particles do not to burn completely (due to insufficient time or temperature), resulting in increased $PM_{2.5}$ concentrations. The spike in emissions when wood is introduced into a combustion region has been observed by others (Bjornsson & Novosselov 2014) This suggests that a batch fed stove, such as a top lit updraft gasifier (TLUD) or continuously fed stove may not exhibit the periodic spikes in emissions observed here resulting in lower overall emissions.

Figure 20b shows the cumulative normalized mass produced, emphasizing the impact the PM spikes have on the total mass produced over a test. Often, the refueling events will produce more PM than the following 2 minutes of steady combustion. Note that the TEOM system is subject to noise because we have reduced the integration time to 10 seconds, and at low levels of PM this noise can result in instantaneous negative mass concentration values. Total mass is integrated over the entirety of the concentration curve, and these negative values do not have an impact on the total mass reported. Longer integration times eliminate these negative values but result in a lower frequency response.

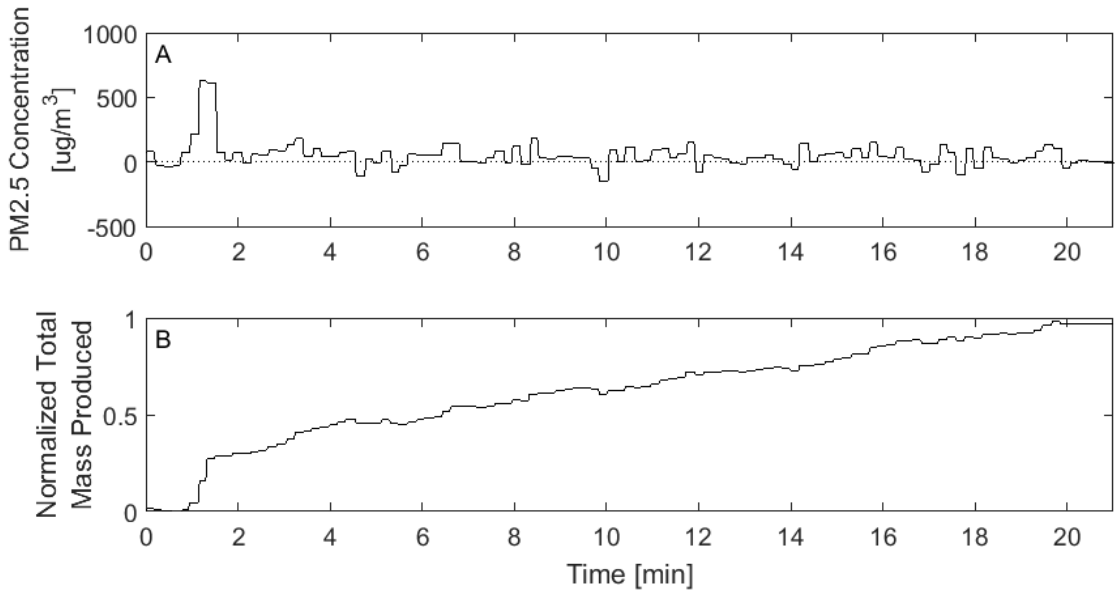

Figure 21: (A) $PM_{2.5}$ concentration from a truncated WBT of a low particulate, UW prototype stove. (B) Normalized cumulative total PM mass produced. Cleaner stoves do not produce much particulate matter during the majority of the burn, which results in the start-up phase $PM_{2.5}$ being a much larger percentage of the total mass produced. Roughly 25% of the total particulate mass is produced in the first two minutes in this test.

Figure 21a depicts a sample test for a University of Washington prototype stove that is designed for low PM emissions. Over a typical WBT the stove produces only 80 mg total $PM_{2.5}$ mass compared to a typical natural draft stove that produces roughly 600 mg. This stove releases low levels of PM once the stove is running at steady state as shown by the average 50 $\mu g/m^3$ PM output compared to 215 $\mu g/m^3$ for the standard natural draft stove. In the sample test shown, over 25% of the total particulate mass produced is from the initial start-up phase, shown as the large peak at 1 minute in Figure 21a and a step increase in cumulative mass in Figure 20b. There are two distinct sections in the test: start-up and normal operating conditions. Once the prototype stove reaches normal operating conditions, the PM production rate remains constant. It should be noted that this is a continuously fed stove, with the operator pushing in an incremental amount of new wood roughly every 10 seconds. It does not exhibit the large spikes associated with

refueling as other stoves do, shown in Figures 20a and 20b. Our measurements suggest that cleaner burning stoves may produce the majority of their $PM_{2.5}$ during initial start-up, when the wood is at a low temperature and there is no char to initially heat the wood, the stove is cold, and when additional combustible material (paper products, kindling etc.) are added to aid in lighting. Standardized testing procedures such as the Water Boil Test typically do not specify lighting techniques, instead suggesting fires be lit according to local practices. Negative instantaneous mass concentrations also appear in Figure 21a due to the increase in noise associated with reduction in the TEOM mass averaging time constant. As stated above, these negative concentrations do not affect the total mass reported.

By modifying the lighting materials/technique used, it is possible to substantially lower the total amount of $PM_{2.5}$ produced. We investigated replacing traditional paper products for lighting with gelled alcohol specifically designed for fire starting. For the traditional start, 20 g wood, 5 g kindling, and 6 g paper towels were burned until the fire died. During the gelled alcohol tests, paper towels were replaced with a liberal amount of gelled alcohol placed directly on the kindling and wood. This was also left to burn until the fire died. Standard WBT procedures were used otherwise. The traditional starts produced an average of 37 mg (±9 mg) $PM_{2.5}$ (n=10), while the alcohol starts produced an average of 15 mg (±4 mg) $PM_{2.5}$ (n=10). The two methods are significantly different, with $p = 0.0016$. This not only shows the importance of fully reporting lighting procedures in results, but it also indicates a specific area for improvement and innovation.

To calculate the differential mass on the filter, the TEOM system uses a calibration constant K_0 that is set by the manufacturer. Pre-weighed filters are inserted into the TEOM during calibration, and the constant is calculated using $\Delta m = K_0 * \left(\frac{1}{f_1^2} - \frac{1}{f_0^2}\right)$ where K_0 is the factory set calibration constant, and f_0 and f_1 are the respective measured frequencies of the filter at some initial time and sometime later (ThermoFisher Scientific 2008). This procedure is repeated five more times. All systems are sold with a certificate of calibration, with the calculated constants listed. The

system used in this work has a calibration constant of 16,363, with a standard deviation for the six calibration tests of ±28.6. This results in an uncertainty of ±0.17% of the total mass reading. The total $PM_{2.5}$ mass produced by the cookstove (mg) as measured by the TEOM system is calculated using Equation 16.

$$m_{PM2.5,TEOM} = \frac{\left((m_f - m_0) * DL * Q_{duct}\right)}{Q_{TEOM} * CF} \quad \text{Eq. 16}$$

Where m_f and m_0 are the reported total masses from the TEOM at the end and start of the test, respectively (µg), DL is the calculated dilution ratio of the external dilution system, Q_{duct} is the flow rate through the hood and ducting system (L/min), Q_{TEOM} is the flow rate required by the TEOM system in liters per minute (3 L/min), and CF is the calculated correction factor. The input variables and their respective uncertainties are listed in Table 12.

Table 12: Uncertainties of TEOM mass variables

Variable	Nominal Value	Uncertainty	Notes
m_f	111.2 µg/115 µg	±0.19 µg/±0.20 µg	The two values are for Tier 4 high power/low power.
m_0	107.7 µg	±0.19 µg	Nominal value comes from real test
DL	18.75	±0.94	Uncertainty was measured over the course of recalibrations
Q_{duct}	5097 L/min	±40.5 L/min	Uncertainty calculated in Chapter 2.1.2
CF	1.49	±0.05	

The values for the TEOM masses (m_f and m_0) come from the Tier 4 $PM_{2.5}$ metrics (high and low power) to determine the uncertainty for the most stringent case. These mass of $PM_{2.5}$ produced at Tier 4 is calculated assuming 1.8 MJ_d for high power and 3.5 L of water and 45 minute simmer

time for the low power metrics. In the high power PM case, the nominal value of the total mass produced is 74.8 mg, with a calculated uncertainty of ±7.4 mg (9.9%). The low power PM has a nominal value of the total mass produced of 157.5 mg, with a calculated uncertainty of ±11.2 mg (7.1%). The full uncertainty calculations are detailed in Appendix A.1.4.

This uncertainty was then compared to the uncertainty associated with the standard gravimetric filter method. The total $PM_{2.5}$ mass produced from the cookstove as measured by the gravimetric filter method is given by

$$m_{PM2.5,Grav} = \frac{\left((m_f - m_0) * Q_{duct}\right)}{Q_{Grav}} \qquad \text{Eq. 17}$$

Where m_f and m_0 are the masses of the filter at the end and start of the test respectively (mg), Q_{duct} is the volumetric flow rate in the ducting (L/min), and Q_{Grav} is the volumetric flow rate through the gravimetric filter housing, set by a sized critical orifice (16.7 L/min). The scale used (AE163, Mettler Toledo, Columbus, OH) has reproducibility of 0.02 mg and readability of 0.01 mg. Table 13 lists the input variables for the total mass calculation for the gravimetric filter method.

Table 13: Uncertainties of gravimetric filter variables

Variable	Nominal Value	Uncertainty	Notes
m_f	0.639685/0.639958 g	±0.02 mg	The two values are for Tier 4 high power/low power.
m_0	0.639447 g	±0.02 mg	Nominal value comes from real test
Q_{duct}	5097 L/min	±40.5 L/min	Uncertainty calculated in Chapter 2.1.2
Q_{Grav}	16.7 L/min	0	Flow set by critical orifice at 16.7 L/min

The values used for m_f and m_0 correspond with equal total mass values compared to the uncertainty analysis for the TEOM system shown above for Tier 4 high and low power $PM_{2.5}$. The

calculated uncertainty for the gravimetric filter method for Tier 4 high power $PM_{2.5}$ (72.7 mg) is ±8.65 mg (11.9%). The uncertainty for Tier 4 low power $PM_{2.5}$ (156 mg) is ±8.72 mg (5.6%). These values are close to the TEOM uncertainty levels, suggesting that the TEOM is equally as uncertain as the standard gravimetric filter method.

We have demonstrated the real-time, quantitative measurement of $PM_{2.5}$ emissions from wood burning cookstoves using a TEOM system. Our work shows that the TEOM requires calibration to the EPA standard gravimetric method because the system is factory calibrated for long-term ambient air environmental monitoring. In our system, the PM concentrations are much higher than that anticipated by the TEOM, which mandates the use of an external dilution system so that accurate PM measurements can be obtained without frequent filter changes. The data show that the corrected TEOM measurements compare well with the standard gravimetric filter method over a wide range of PM emission rates and are independent of several emission system modifications (e.g. internal sample cell temperature, with and without sample desiccation). The TEOM system provides real-time quantitative data that can used to understand transient particulate emission events such those that occur when refueling or at stove lighting. We showed that refueling is a major contributor to overall PM emissions, with 37% of PM being produced during refueling for a typical cookstove. We also showed that initial startup can also play a large role in PM production (e.g. 25%), especially in cleaner stoves that produce lower levels of PM during normal operation. Once set up and calibrated, the TEOM system allows for more rapid stove testing and eliminates filter gravimetric filter changes between the high power and simmer phases of WBTs. Time-resolved particulate data enables stove designers to have insight into the events and parameters that influence particulate matter production. This insight may enable a more rapid assessment of how stove design and operation impacts performance and allow more rapid turnaround of prototype designs. The TEOM system provides time-resolved, quantitative PM emission data that is otherwise unavailable, and is proving to be a valuable tool in cookstove development.

Chapter 4: Excess Air Estimation Measurements

In this chapter, a method for measuring the excess air of a cookstove is presented, as well as methods for estimating the flow rates through the cookstove. It is generally accepted that natural draft stoves draw significant excess air, though we are not aware of any methods to quantify it. Understanding excess air is important, as it is critical to stove performance including mixing, PM production, as well as heat transfer and thermal efficiency.

4.1 Experimental Setup for Excess Air

We use a Burn Design Lab side fed, natural draft wood-fed cookstove, shown in Figure 22. The stove is 33 cm tall and 28 cm in diameter, with an 11 cm x 12 cm rectangular feed tunnel on one side for fueling. This feed tunnel extends towards the central vertical riser, which directs the hot combustion gases upward towards the top. The stove is equipped with a pot skirt, which keeps the hot gases in contact with the vertical surface of the pot. The stove used here is the same stove used in Chapter 3 (with the addition of a pot skirt), where detailed stove dimensions are listed. An identical stove with an added door over the feed tunnel is used for excess air comparison**.**

To calculate the amount of excess air, we sample the combustion gases from the top of the pot skirt from four locations (front, right side, left side, back) as the cookstove flow field is not necessarily axisymmetric. This is done with a four-pronged rake made from 3/16” OD stainless steel tubing, shown in Figure 23. The sample inlets are positioned and taped at the top of the pot skirt. In the case of a stove without a pot skirt, the sample inlets can be positioned at the gap between the pot and the top of the stove, near the bottom edge of the pot. It is important to position the sample inlets such that only combustion gases are sampled. The stainless steel tubing is connected to ¼” OD PVC tubing and converges into a single sample line.

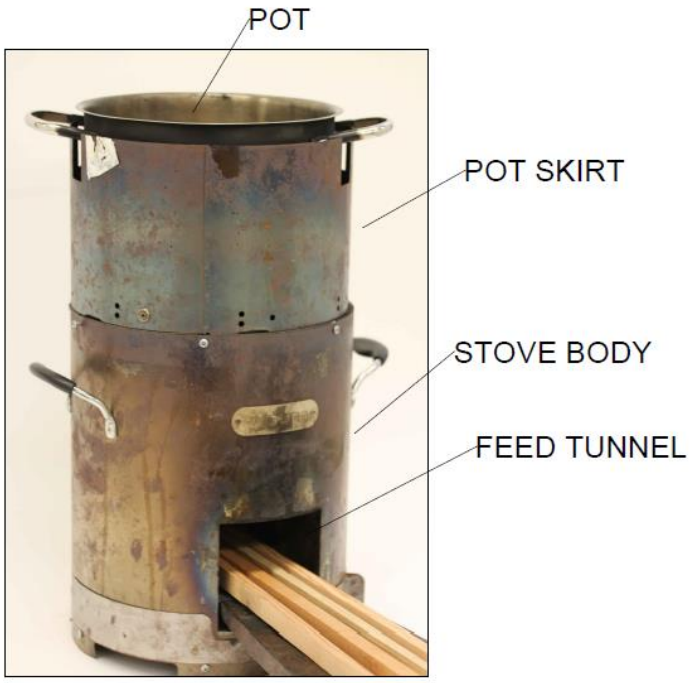

Figure 22: Burn Design Lab side fed, natural draft wood stick cookstove used. The pot skirt sits on top of the stove body to keep the combustion gases in contact with the pot. The pot sits inside of the pot skirt, with an 8 mm gap between the pot body and the pot skirt. An identical stove with an added vertical door over the feed tunnel is used for excess air comparison.

Each sample inlet is assumed to draw an equal flow. The flow is drawn by a bellows pump (MB-158, Metal Bellows, Sharon, MA) to a CO_2 analyzer (PIR-2000, Horiba, Kyoto, Japan). The real-time mass of the cookstove is measured using a digital scale (ABK 70a, Adam Equipment, Danbury, CT). The CO_2 concentration and stove mass are recorded with a LabView based data acquisition system. During a test, the cookstove is run according to the Water Boil Test (WBT) guidelines. Five liters of water is brought to a boil from room temperature, and then kept within 5 °C of local boiling temperature for 45 minutes. The cookstove is operated at several different fire powers by adjusting the wood feed rate during the simmer portion of the test to fully characterize the stove, with the firepower held as close to constant as possible during each sampling period.

Figure 23: Experimental setup for measuring excess air within a natural draft cookstove. Four 3/16" OD stainless steel sampling probes are positioned and taped in a diamond configuration at the top of the pot skirt, so that they sample the combustion gases in the gap between the pot and the pot skirt. These sample lines then converge to a single sample line which is connected to a CO_2 analyzer.

A lid is used to minimize water evaporation that may bias the measurement of instantaneous firepower from the time varying stove mass.

Only data after the water has reached boiling point are considered, as the stove heating up and approaching steady-state operating conditions may affect emissions characteristics. Low stove temperatures may affect the combustion by lowering the gas temperature, leading to incomplete combustion and an increase in incomplete combustion products, affecting CO_2 production as well. After the test is completed, the data are visually screened for timespans of constant CO_2 output. An example of the CO_2 concentrations during an excess air test is shown in Figure 24.

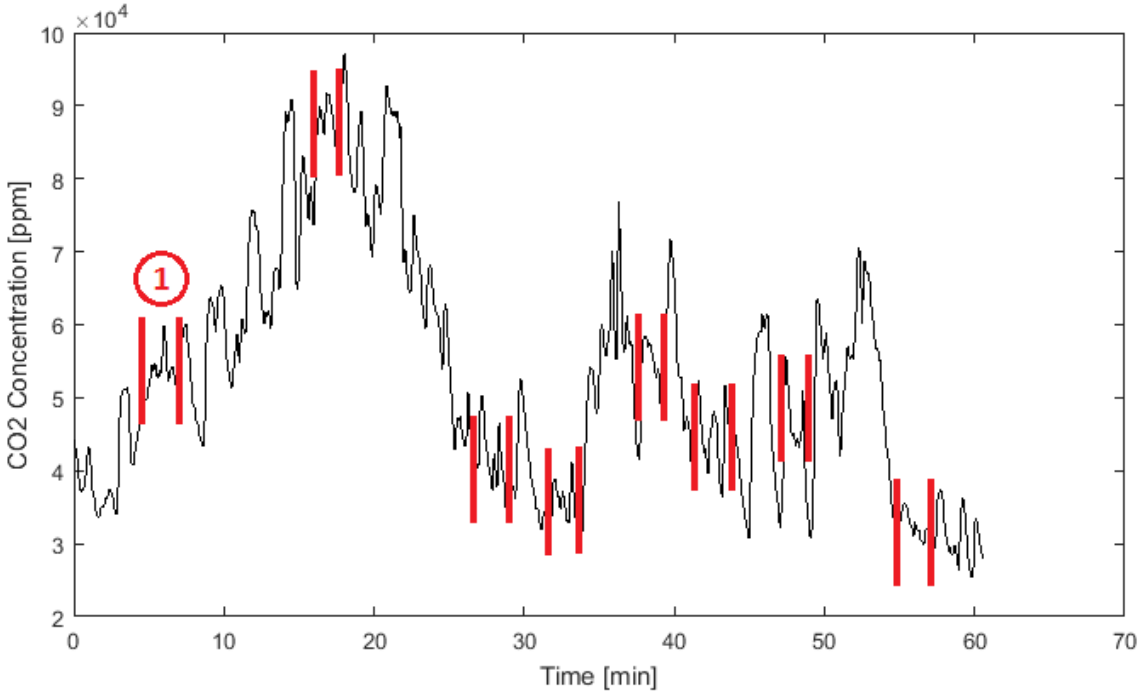

Figure 24: CO_2 concentrations from a sample excess air test. The sampling periods used are shown in between the red bars. During the test, the firepower of the stove is varied over a range to fully characterize the stove. The CO_2 concentration is sampled and recorded using the sampling probes positioned in between the pot and the pot skirt. The concentration data is then visually screened for periods of roughly constant CO_2 concentrations, and the concentration averages over these periods are calculated. The section labeled 1 is used for the sample calculation detailed below.

The timestamps of constant CO_2 regions are recorded, and the CO_2 concentration is averaged over each timespan. The combustion gas velocities exiting the stove at each of the sampling points are assumed to be equal. Varying velocities would require separate monitoring for each sampling point, and a weighting scheme to average the four sampling points to account for the different mass flow rates. An ultimate analysis of Douglas Fir wood (Kobayashi et al. 2009) is used in calculating the air-fuel equivalence ratio (φ), shown in Table 13.

Table 14: Ultimate analysis of Douglas Fir wood

Species	moles per gram of wood
C	0.0419
H	0.0635
N	0.0001
O	0.0269

The balanced combustion equation,

$$C_xH_yO_z + \varphi\left(x+\frac{y}{4}-\frac{z}{2}\right)(O_2+3.76N_2) \rightarrow xCO_2+\frac{y}{2}H_2O+3.76\varphi\left(x+\frac{y}{4}-\frac{z}{2}\right)N_2+(\varphi-1)\left(x+\frac{y}{4}-\frac{z}{2}\right)O_2 \quad \text{Eq. 17}$$

is used to write an equation for the CO_2 concentration as a function of the air-fuel equivalence,

$$y_{CO2}=\frac{moles\ of\ CO_2}{moles\ of\ total\ products}=\frac{x}{x+\frac{y}{2}+3.76\varphi\left(x+\frac{y}{4}-\frac{z}{2}\right)+(\varphi-1)\left(x+\frac{y}{4}-\frac{z}{2}\right)} \quad \text{Eq. 18}$$

where x,y, and z are the moles of carbon, hydrogen, and oxygen respectively per gram of wood from the ultimate analysis shown in Table 13. y_{CO2} is the average measured CO_2 concentration over the sampling period. The numerator is the moles of CO_2 (x) present in the products, while the denominator is the moles of total products. It is assumed that all of the carbon present in the fuel is converted to CO_2. As the measured average CO_2 concentration is known, the only unknown in Eq. 18 is the air-fuel equivalence ratio (φ). The air-fuel equivalence ratio is then solved for, and excess air is then calculated ($Excess\ Air = \varphi - 1$). This process is repeated for each sampling period of constant CO_2. A sample calculation is done for the section labeled 1 in Figure 24. The average CO_2 concentration over the sampling period is 51,800 ppm. This is used in Eq. 18, shown below in Eq. 19 with the variables replaced by the values used. During this sampling period, 58 grams of wood were consumed over 4.42 minutes with a firepower of 4.23 kW.

$$\frac{51800}{1000000} = \frac{0.0419}{0.0419 + \frac{0.0635}{2} + 3.76\varphi\left(0.0419 + \frac{0.0635}{4} - \frac{0.0269}{2}\right) + (\varphi - 1)\left(0.0419 + \frac{0.0635}{4} - \frac{0.0269}{2}\right)}$$

Eq. 19

$$\varphi = 3.71$$

4.2 Cookstove Flow Rates Estimations

The data in the excess air estimations can be subsequently used to estimate the both the total and air molar flow rates through the cookstove. The total molar flow rate through the stove, which is the sum of the air entering the stove and the combustion products produced, can be estimated using the real-time mass scale and CO_2 concentrations. Assuming all of the carbon present in the wood is converted to CO_2, the molar production rate of CO_2 can be estimated using Equation 19.

$$\dot{n}_{CO2} = \Delta m * \frac{0.0419}{t} \qquad \text{Eq. 19}$$

Where $\dot{n}_{CO_2}$ is the molar production rate of CO_2 (mol/s), Δm is the mass of wood consumed over the averaging period (g), 0.0419 is the moles of carbon per gram of wood (see Table 13), and t is the duration of the averaging period (s). The molar production rate of CO_2 can then be used to estimate the total molar flow rate of the combustion products exiting the stove using the definition of gas concentration, assuming all of the combustion gases are ideal,

$$\frac{\dot{n}_{CO2}}{y_{CO2}} = \dot{n}_{total} \qquad \text{Eq. 20}$$

Where $\dot{n}_{CO_2}$ is the molar production rate of CO_2 (mol/s), y_{CO2} is the measured CO_2 concentration from the excess air test, and $\dot{n}_{total}$ is the total molar production rate of products from combustion (mol/s), which is the sum of the right-hand side of Eq. 17.

Using the estimated air-fuel ratio and the wood consumption rate, the air flow rate through the stove can be estimated as well. This calculation is important to determine the velocity of the air

entering the stove and how it compares to the hood face velocity. If the hood face velocity is not significantly smaller than the stove face velocity, the cookstove operation may transition to a pseudo-forced draft regime, impacting cookstove performance results. The left side of Eq. 17 is used in this calculation. The moles of air entering the stove is represented by the coefficient in front of the oxygen/nitrogen term ($\varphi\left(x+\frac{y}{4}-\frac{z}{2}\right)(O_2+3.76N_2)$). As the air-fuel equivalence ratio is now known, this coefficient can be calculated. The moles of oxygen and nitrogen can be combined to give the moles of air, assuming other gases present are negligible, resulting in a coefficient of $\varphi\left(x+\frac{y}{4}-\frac{z}{2}\right)(4.76Air)$). This coefficient is then multiplied by the feed rate of wood in grams per second, determined by the real-time scale. This moles of air entering the stove is given by Equation 21.

$$\dot{n}_{air}=\dot{m}_{wood}*\ \varphi\left(x+\frac{y}{4}-\frac{z}{2}\right)(4.76) \qquad \text{Eq. 21}$$

The molar flow rate of the air can then be converted into a volumetric flow rate of the air entering the stove, which can then converted into a linear velocity of the air assuming that the air behaves as an ideal gas and that the velocity over the stove face area is constant. This face velocity is unique to each stove as the area in which the air flows through is unique to each stove. The stove without a door used here (shown in Figure 22) has an air flow rate of roughly 0.267 mol/s (6.44 L/s) through the stove. The stove's feed tunnel where air enters has an area of 121 cm^2. The volumetric flow rate corresponds to a linear stove face velocity of 0.53 m/s. This value can then be compared to the hood face velocity, which is calculated to be 0.11 m/s for the testing suite installed at the University of Washington (calculated in Chapter 2.1.1). If multiple stoves are to be tested, the stove with the minimum face velocity should be used for comparison to the hood face velocity. While there is no general rule for the ratio of stove/hood face velocities, the hood face velocity should not exceed 0.25 m/s (Aprovecho 2013, Jetter et al. 2012).

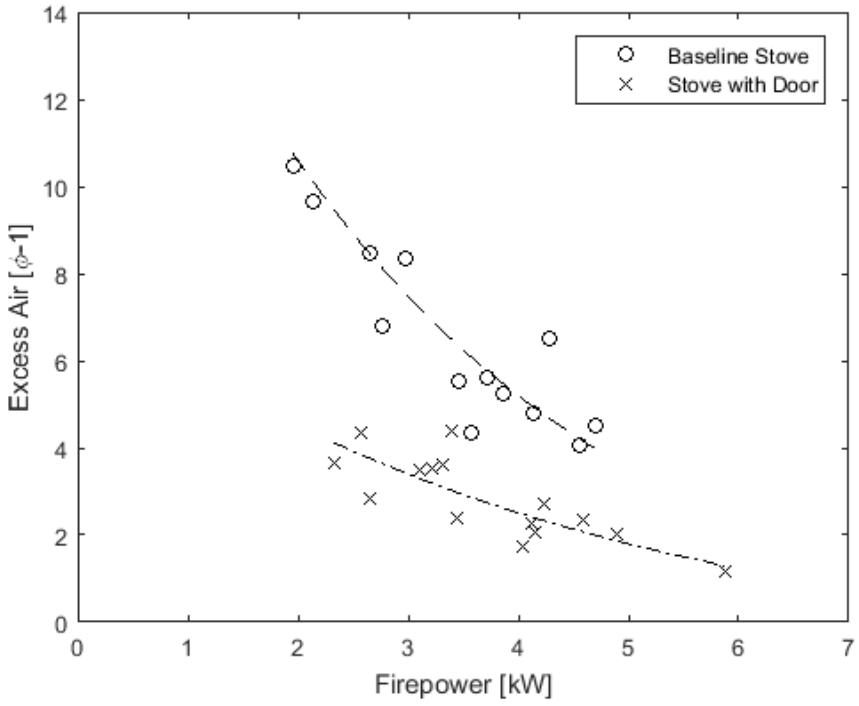

Figure 25: Excess air as a function of firepower for a BURN Design Lab stove prototype with and without an added door over the feed tunnel. The excess air decreases as firepower increases, as more volatiles are produced at higher firepowers allowing less air into the cookstove. At low firepowers (2 kW), there is almost twelve times the stoichiometric amount of air in the baseline stove. The addition of a door in the feed tunnel reduced the amount of excess air present by nearly 33% at 4 kW.

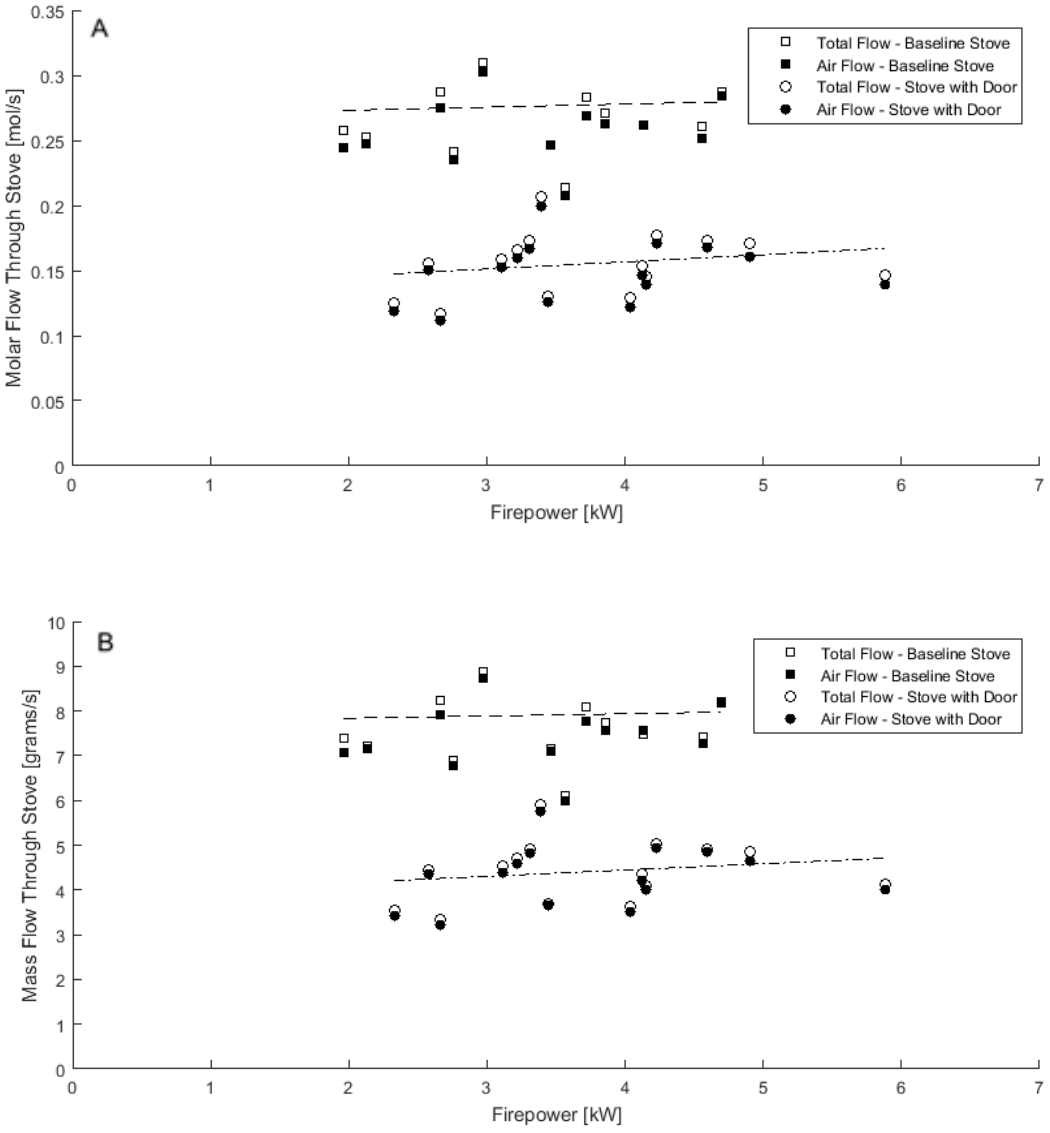

Figure 26: A) Total and air molar flow rates through the stove for a BURN Design Lab stove and a stove with an added door over the feed tunnel. The molar flow rates through the stoves are roughly constant, regardless of firepower. The addition of a door over the feed tunnel decreases the total molar flow rate through the stove. The total flow is slightly higher than the air flow rates due to the addition of gaseous combustion products. The trend lines shown are for the total flow rates. B) Total and air mass flow rates through the stoves. This shows a very similar trend compared to the molar flow rates.

4.2 Results and Discussion of Excess Air Estimations

Several tests were performed to characterize the excess air present in the stove over a range of firepowers. In the baseline cookstove design, the feed tunnel is unobstructed, allowing air to flow into the stove freely. We also tested the same stove after adding a vertical door over the feed tunnel, blocking the majority of the area while allowing sticks to be fed into the combustion chamber. Figure 25 shows the excess air for the stoves as a function of the firepower.

There is a strong relationship between excess air and firepower. As firepower increases, the amount of excess air present in the cookstove decreases. At low firepowers (2 kW) in the baseline stove, there is nearly twelve times the necessary (stoichiometric) air. This decreases to nearly six times the necessary air at firepowers near 4 kW.

The addition of a door results in a decrease in the amount of excess air present, as shown in Figure 25. At 4 kW, the amount of excess air through the stove with an added door is roughly four times the necessary air, a decrease of 33% compared to the baseline stove without a door. Additional testing of the stove with the door has shown that the door results in greater thermal efficiency and shorter time to boil, which is likely due to a decrease in excess air as well as a decrease in radiative losses out of the feed tunnel.

Figure 26 shows the molar flow rate through the stoves as a function of the fire power. It is important to note that the total molar flow rate is the flow rate of the combustion gases exiting the cookstove, while the air molar flow rate is the flow rate of the air entering the cookstove. This data shows that both the molar and mass flowrates remain roughly constant. This is explained by using Bernoulli's equation in a sample situation to calculate the mass flow of air through a vertical pipe which can approximate a cookstove. The mass flow of air through a chimney 0.3 m tall for varying exit air temperatures is shown in Figure 27a, with an enlarged view for the temperatures that correspond to cookstove exit gas temperatures shown in Figure 27b.

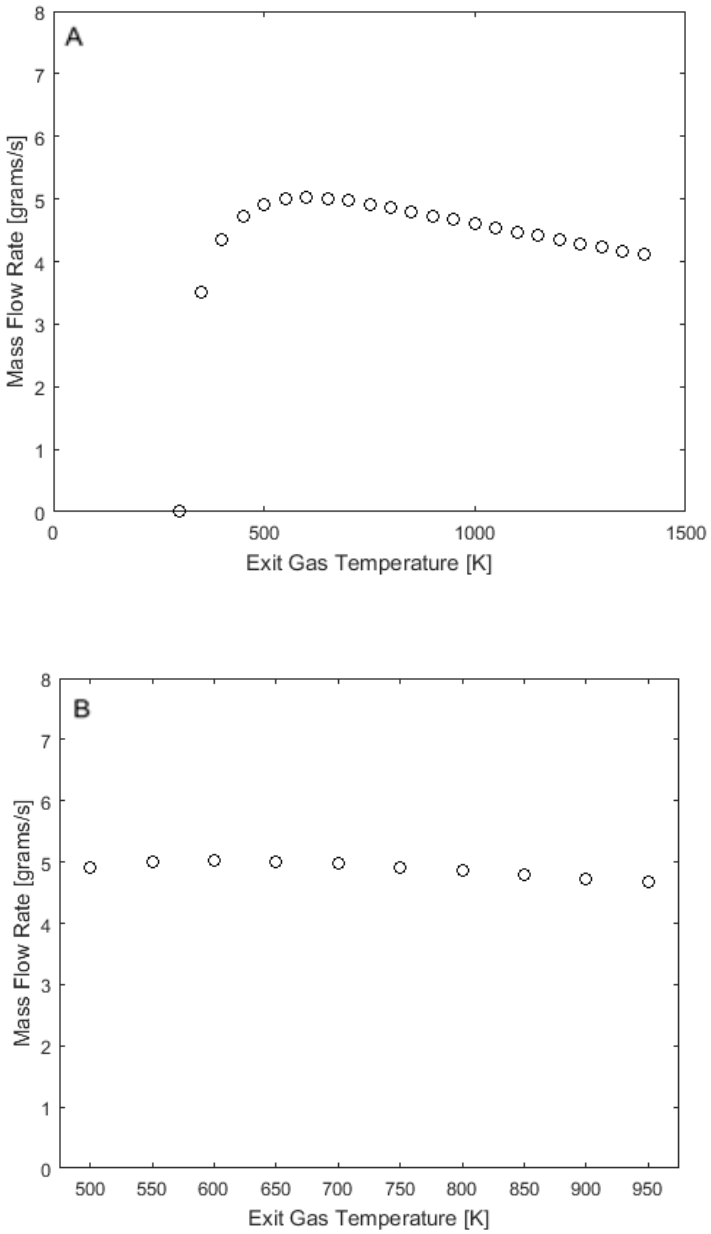

Figure 27: Air mass flow through a chimney 0.3m tall using Bernoulli's Equation for a range of exit gas temperatures. As this is an extremely simplified model of stove operation, the values presented are not meant to be representative of actual stove operation. A) The mass flow over a wide range of temperatures shows a sharp increase in flow followed by a steady decrease, caused by the decreasing air density as temperature increases. B) The air mass flow over exit gas temperatures that have been recorded during testing using thermocouples. The mass flow through the chimney remains roughly constant between 500 and 950K.

The calculations for these plots can be found in Appendix A.2. At typical cookstove exit gas temperatures, the total mass flow rate through the stove remains roughly constant. While the velocity of the air increases, the density decreases due to the increasing temperature, which results in a near constant mass flow rate.

This result helps to explain the decrease in the excess air as firepower increases. As firepower increases, the stoichiometric requirements for combustion increase as well, and the amount of air present that is in excess decreases even as the amount of total air present remains constant. The addition of a door over the feed tunnel results in a decrease in total flow through the stove by nearly 37%. The offset between the total molar flow rate and the air flow rate should be constant, calculated by using the balanced combustion equation (Eq. 17) and subtracting the number of moles of air (O_2+N_2) from the total number of moles of products. The calculated offset is $\frac{y}{4}+\frac{z}{2}$ where y and z are the number of moles of hydrogen and oxygen present in the fuel per gram, respectively. This constant offset is not seen in Figure 26, as the assumptions of completely uniform wood and complete combustion to CO_2 lead to experimental inaccuracies. The mass flow rates shown in Figure 26 should also show a diverging behavior between the total and air mass flow rates as firepower increases, due to the increased mass of the combusted fuel. This is not seen in Figure 26. This may be due to insufficient accuracy of this method to resolve these slight differences in flow rates. At a firepower of 1 kW, with φ calculated from the curve fit in Figure 25 for the stove without a door, the mass rate of wood is 1% of the total mass entering the stove, with the remaining 99% consisting of entering air. At a firepower of 7 kW, the percentage of mass entering the stove given by the wood increases to 6.4%. While this protocol allows for estimation of the flow rates and amount of excess air present, we stress that it is strictly as estimation due to the assumptions made, and is not accurate enough to resolve these small differences in flow rates.

While large amounts of excess air may lead to more complete combustion, additional unused excess air cools the combustion gases, leading to decreased heat transfer to the pot. This results in lower overall thermal efficiencies and longer times to boil, both undesirable traits in a cookstove.

4.3 Summary

We have demonstrated a procedure for experimentally estimating the excess air flowing into a wood-fed natural draft cookstove. This measurement can be a valuable tool for cookstove development and designers by providing details on the the flow of air that impacts the combustion and heat transfer in the stove. We showed that the amount of excess air present decreases with firepower, while the total and air molar flow rates through the stove remains roughly constant. We also showed that the addition of a door in the feed tunnel decreases the amount of excess air present by roughly 33% at a firepower of 4 kW and later testing shows that the addition of a door also has beneficial effects on overall thermal efficiency and time to boil.

Chapter 5: Uncertainties for ISO/IWA Comparison Metrics

In this chapter, the uncertainties for the ISO/IWA comparison metrics are calculated using previously calculated uncertainties for the numerators/denominators (detailed throughout this thesis). This fully characterizes the uncertainty of the cookstove comparison testing suite installed at the University of Washington.

5.1 ISO/IWA Comparison Metrics Uncertainty Calculations

Table 14 lists the Tier 4 ISO/IWA comparison metrics input variables along with the necessary calculation and relevant uncertainties.

Table 15: Uncertainties for ISO/IWA comparison metrics input variables

ISO/IWA Metric	Calculation	Input Variables	Nominal Value	Uncertainty	Notes
High Power CO (g/MJ$_d$)	$CO_{HP} = \frac{g_{CO}}{MJ_d}$	g_{CO}	14.5 g	±0.9 g	Section 3.2.1
		MJ_d	1.8 MJ	±0.01 MJ	Section 3.3.1
Low Power CO (g/min/L)	$CO_{LP} = \frac{g_{CO}}{min * L}$	g_{CO}	14 g	±0.9 g	Nominal value assumes Tier 4, 3.5 L, and 45 minute simmer
		min	45 min		
		L	3.5 L	±0.001 L	Uncertainty determined by scale
High Power PM$_{2.5}$ (mg/MJ$_d$)	$PM_{HP} = \frac{mg_{PM}}{MJ_d}$	mg_{PM}	74.9 mg	±7.4 mg	Section 4.3
		MJ_d	1.8 MJ	±0.01 MJ	Section 3.3.1
Low Power PM$_{2.5}$ (mg/min/L)	$PM_{LP} = \frac{mg_{PM}}{min * L}$	mg_{PM}	157.5 mg	±11.2 mg	Nominal value assumes Tier 4, 3.5 L, and 45 minute simmer
		min	45 min		
		L	3.5 L	±0.001 L	Uncertainty determined by scale
High Power Thermal Efficiency (%)	$\eta_{HP} = \frac{MJ_d}{MJ}$	MJ_d	1.8 MJ	±0.01 MJ	Section 3.3.1
		MJ	4 MJ	±0.04 MJ	Section 3.3.1

Low Power Specific Consumption (MJ/L/min)	$\eta_{LP} = \frac{MJ}{min * L}$	MJ	2.7. MJ	±0.04 MJ	Nominal value assumes Tier 3, 3.5 L, and 45 minute simmer
		min	45 min		
		L	3.5 L	±0.001 L	Uncertainty determined by scale
Indoor Emissions CO	$IE_{CO} = \frac{g_{CO}}{min}$	g_{CO}	14 g	±0.9 g	Section 3.2.1
		min	45 min		
Indoor Emissions $PM_{2.5}$	$IE_{PM} = \frac{mg_{PM}}{min}$	mg_{PM}	90 mg	±8 mg	Section 3.2.1
		min	45 min		

The uncertainties for all eight Tier 4 ISO/IWA comparison metrics were calculated. Table 15 lists the results.

Table 16: Uncertainties for Tier 4 ISO/IWA comparison metrics

ISO/IWA Metric	Nominal Value	Uncertainty
High Power CO (g/MJ_d)	8 g/MJ_d	±0.5 g/MJ_d (6.3%)
Low Power CO (g/min/L)	0.09 g/min/L	±0.006 g/min/L (6.7%)
High Power $PM_{2.5}$ (mg/MJ_d)	41.6 mg/MJ_d	±4.1 mg/MJ_d (9.7%)
Low Power $PM_{2.5}$ (mg/min/L)	1 mg/min/L	±0.07 mg/min/L (7%)
High Power Thermal Efficiency (%)	45%	±0.5% (1.3%)
Low Power Specific Consumption (MJ/min/L)	0.017 MJ/min/L	±0.0003 MJ/min/L (1.2%)
Indoor Emissions CO (g/min)	0.31 g/min	±0.02 g/min (6.5%)
Indoor Emissions $PM_{2.5}$ (mg/min)	2 mg/min	±0.18 mg/min (12.6%)

The full uncertainty calculations are detailed in Appendix A.1.5. The nominal values in Table 15 represent the Tier 4 metrics, which are the most stringent cases and sub-Tier 4 results have lower uncertainties than those listed.

Chapter 6: Conclusions and Future Work

To design better performing cookstoves, a well-developed cookstove emissions and performance testing suite is required to quantitatively test and compare cookstoves as well as to better understand underlying cookstove dynamics and physics. In this thesis, a complete cookstove emissions and performance testing suite is described. The suite is comprised of an emissions hood and ducting to capture all of the gaseous and particle emissions from the cookstove, NDIR CO and CO_2 analyzers to characterize gaseous emissions concentrations, and a time-resolved particulate matter analyzer. A real-time mass scale is also used to determine instantaneous firepowers during cookstove operation. The testing suite is designed for quantitative comparison of cookstoves using standardized laboratory testing protocols such as the Water Boil Test. The system components are chosen to minimize uncertainty, which is calculated for the individual components, as well as the ISO/IWA comparison metrics. Design decisions, such as tradeoffs between competing analysis techniques and methodologies are also discussed.

An innovative time-resolved particulate matter analyzer (TEOM) has been successfully applied to cookstove analysis. This thesis describes several modifications (both internal and external) that were necessary due to the TEOM's original design use of ambient air monitoring. These changes include user-adjusted internal programming to increase an internal rolling averaging function, as well as an external dilution system, as the particle concentrations experienced in cookstove analysis are much higher than those in ambient air monitoring. Other challenges to successful TEOM application, such as pressure concerns are also discussed. A comprehensive comparison was performed to a standardized gravimetric method and the TEOM was found to overestimate the total mass measurement in comparison to the standardized gravimetric method. A correction factor of 1/1.49 was calculated and applied to the TEOM mass measurement the two methods into agreement. The TEOM system allows researchers to better understand cookstove dynamics

in real-time with direct PM analysis, aiding in stove design and development. Several applications of the TEOM were discussed, such as the particulate matter produced at start-up and refueling events. It was found that transient high PM events caused by refueling significantly contribute to the overall total $PM_{2.5}$ mass produced over the duration of a test. It was also found that the start-up phase can produce relatively large amounts of particulate matter, especially in cleaner burning stoves. This information, which would not otherwise be available to researchers, suggests specific areas for improvement and innovation.

A process for experimentally estimating the excess air present in a natural draft cookstove is developed. While it is well-known in the cookstove community that there is a significant amount of excess air present in natural draft cookstove, this is the first time a method has been disclosed to quantitatively estimate the excess air. This estimate enables researchers to better understand the environment inside cookstoves, specifically the heat transfer and combustion characteristics, which can be used to guide design. This excess air procedure was then applied to a cookstove with and without an added door over the feed tunnel. It was found that at medium firepowers (4 kW), there is nearly six times the required stoichiometric air present in the cookstove without the door. When a door is added over the feed tunnel, the air flow through the stove decreases to four times the required stoichiometric air. Later investigations show that the added door is beneficial to overall thermal efficiencies, potentially due to the decrease in excess air present. It was also found that the air and total flow rates through the stove are roughly constant regardless of firepower.

As mentioned above, the uncertainties of the cookstove emissions and performance testing suite were calculated for each ISO/IWA tiered metric. It was shown that the described system has uncertainty below 10% for all of the comparison metrics. These uncertainties were calculated for the most stringent cases (Tier 4) for emissions metrics and for typically seen values for thermal efficiency metrics. As cookstove comparison tests are already prone to large deviations between

tests (mostly due to operation variations as well as heterogeneous wood characteristics), minimizing uncertainty is extremely important to determine the impact of stove morphologies.

Current standardized laboratory testing results significantly differ from in-field measurements. It is thought that this is primarily due to difference in stove operation, such as fuel quality or user actions. Work is currently being conducted at the University of Washington to develop a stress test in which cookstoves are evaluated using a wide range of fuels and operating conditions. Fuel size and moisture content is varied, as well as tending times and firepower. The goal of the stress test is to better represent in-field usage through a variety of conditions to better predict real-world performance and emissions metrics.

As the discrepancy between the TEOM and gravimetric filter method discussed in this work is not fully understood, additional work may be performed to ascertain the cause. Meyer et al. (2008) suggest that the presence of electrically charged particles influence reported mass of the TEOM system, leading to an overestimation of mass. Investigating the properties of particulate matter from the duct more thoroughly may lead to a better understanding of the correlation between the TEOM and gravimetric filter method.

Improved cookstoves remain one of the best solutions to a serious global health and climate change issue. By developing more robust testing methodologies and testing systems, and by utilizing more analytical tools to better understand cookstove operation and dynamics, we can design better performing cookstoves, helping billions of people and changing the world for the better.

Appendix

A.1 Uncertainty Calculations

This section details the uncertainty calculations. Equation 4 (shown below as Eq. A.1) is applied to each system of the cookstove emissions and performance testing suite to calculate the associated uncertainty, where M denotes the calculated metric, X and Y represent input variables on which M is dependent, and δX and δY represent uncertainties associated with X and Y, respectively. The calculations are organized by main text section.

$$\delta M = \sqrt{\left(\frac{\partial M}{\partial X} * \delta X\right)^2 + \left(\frac{\partial M}{\partial Y} * \delta Y\right)^2 + \cdots} \quad \text{Eq. A.1}$$

A.1.1 Hood and Ducting Uncertainty

The global equations used to calculate hood and ducting flow rates are as follows, with Eq. A.2 is used to calculate the volumetric flow rate in the ducting (L/min), and Eq. A.3 is used to calculate the molar flow rate (mol/s) in the ducting.

$$Q = K * \sqrt{\Delta P} * 28.3168 \quad \text{Eq. A.2}$$

$$\dot{n}_{duct} = Q * \left(\frac{101.41}{286.9 * (T_a + 273.15)}\right) * \frac{1000}{60 * 28.97} \quad \text{Eq. A.3}$$

In Equation A.2, ΔP is the differential pressure measured by the diamond flow sensor in the ducting, K is the K-factor calibration constant, listed as 455 by the manufacturer, and 28.3168 is the conversion from cfm to L/min. In Equation A.3, Q is the volumetric flow rate calculated by Equation A.2, 101.41 is the ambient pressure (kPa), 286.9 is the specific gas constant for air

(J/kg/K), T_a is the ambient temperature (°C), and 28.97 is the molar mass of air (g/mol). The input variables and values are listed below.

Variable	Nominal Value	Uncertainty	Notes
K	455	0	Nominal value given by manufacturer
ΔP	0.158" w.g.	±0.0025" w.g. (1% of full scale - set at 0.25" w.g.)	Uncertainty determined by pressure transducer.
T_a	21 °C	±0.1575 °C (±0.75% of reading)	

The uncertainty equations for the volumetric flow rate in the ducting (Eq. A.2) are shown below.

Equation	Value	Equation
$\frac{\partial Q}{\partial K} = \sqrt{\Delta P} * 28.3168$	11.26	Eq. A.4
$\frac{\partial Q}{\partial P} = 14.1584 * \frac{K}{\sqrt{P}}$	16206.79	Eq. A.5
$\delta Q = \sqrt{\left(\frac{\partial Q}{\partial K} * \delta K\right)^2 + \left(\frac{\partial Q}{\partial P} * \delta P\right)^2}$	40.5 L/min	Eq. A.6

The uncertainty of the volumetric flow rate through the ducting is ±40.5 L/min. The uncertainty equations for the molar flow rate in the ducting (Eq. A.3) are shown below.

Equation	Value	Equation
$\frac{\partial \dot{n}_{duct}}{\partial Q} = \frac{0.203353}{T_a + 273.15}$	0.000691	Eq. A.7
$\frac{\partial \dot{n}_{duct}}{\partial T_a} = -0.20335 * \frac{Q}{(T_a + 273.15)^2}$	0.01198	Eq. A.8
$\delta \dot{n}_{duct} = \sqrt{\left(\frac{\partial \dot{n}_{duct}}{\partial Q} * \delta Q\right)^2 + \left(\frac{\partial \dot{n}_{duct}}{\partial T_a} * \delta T_a\right)^2}$	0.03 mol/s	Eq. A.9

The uncertainty of the molar flow rate through the ducting is ±0.03 mol/s.

A.1.2 CO Uncertainty

The global equation used to calculate total grams of CO produced over the duration of a test is as follows:

$$g_{CO} = \sum_{t_0}^{t_{final}} \frac{x_{CO}}{1000000} * \dot{n}_{duct} * 28.01 * \Delta t \qquad \text{Eq. A.10}$$

Here, x_{CO} is the concentration of CO (ppm), 28.01 is the molar mass of CO (g/mole), $\dot{n}$ is the total molar flow rate in the duct calculated by Eq. A.3, and Δt is the length of time step (2 seconds), over which it is assumed the measured concentrations and flow rates remain constant. The grams of CO produced during each time step are then summed over the entirety of the test to give the total grams of CO produced. The input variables and values are listed below.

Variable	Nominal Value	Uncertainty	Notes
x_{CO}	165 ppm	±5 ppm (0.5% of full scale – set at 1,000 ppm)	
$\dot{n}_{duct}$	3.48 moles/s	±0.03 moles/s	Uncertainty calculated in Section A.1.1
Δt	2 sec	0	

The uncertainty equations for an individual time step using Eq. A.10 are shown below.

Equation	Value	Equation
$\frac{\partial g_{CO}}{\partial x_{CO}} = 0.00002801 * \dot{n}_{duct} * \Delta t$	0.00020	Eq. A.11
$\frac{\partial g_{CO}}{\partial \dot{n}_{duct}} = 0.00002801 * x_{CO} * \Delta t$	0.0092	Eq. A.12
$\frac{\partial g_{CO}}{\partial \Delta t} = 0.00002801 * x_{CO} * \dot{n}$	0.0161	Eq. A.13
$\delta g_{CO} = \sqrt{\left(\frac{\partial g_{CO}}{\partial x_{CO}} * \delta x_{CO}\right)^2 + \left(\frac{\partial g_{CO}}{\partial \dot{n}_{duct}} * \delta \dot{n}_{duct}\right)^2 + \left(\frac{\partial g_{CO}}{\partial \Delta t} * \delta \Delta t\right)^2}$	0.001 g	Eq. A.14

The uncertainty of each time step is summed over the duration of a test, assumed to be 30 minutes (900 time steps), to give a total uncertainty of ±0.9 g. This is the uncertainty associated with Tier 4 high-power CO.

A.1.3 Mass Scale Uncertainty

The global equations used to calculate mass variables are as follows:

$$MJ_d = \frac{\left(4.179 * m_{water,0} * \frac{T_{water,f} - T_{water,0}}{1000}\right) + \left(2257 * \frac{m_{water,0} - m_{water,f}}{1000}\right)}{1000} \quad \text{Eq. A.15}$$

$$MJ = \frac{m_{wood,eqv.} * HV_{wood}}{1000000} \quad \text{Eq. A.16}$$

$$m_{wood,eqv.} = \frac{m_{wood} * \left(HV_{wood} * (1 - mc) - \left(mc * 4.186 * \left(T_{water,f} - T_a\right) + 2257\right)\right) - m_{char} * HV_{char}}{HV_{wood}} \quad \text{Eq. A.17}$$

Eq. A.15 is used to calculate the megajoules of energy delivered to the pot, and Eq. A.16 is used to calculate the megajoules of energy produced by the wood. Eq. A.17 calculates the equivalent grams of wood consumed, taking into account moisture content and char production. This value is then used in Eq. A.16. In these equations, m_{water} is the mass of the water (kg), T_{water} is the temperature of the water (°C), T_a is the ambient temperature (°C), $m_{wood,eqv.}$ is the equivalent mass of fuel consumed (g), HV is the heating value of the wood and char (kJ/kg), m_{wood} is the measured mass of fuel consumed (g), mc is the percent moisture content of the wood, and m_{char} is the mass of char produced (g). Subscripts 0 and f denote measurements taken at the start and end of the test, respectively. The input variables and values are listed below.

Variable	Nominal Value	Uncertainty	Notes
$m_{water,0}$	5,000 g	±1 g	
$m_{water,f}$	4,940 g	±1 g	
m_{wood}	240 g	±1 g	
m_{char}	5 g	±1 g	
$m_{wood,eqv.}$	208 g	±2.1 g	Uncertainty calculated
$T_{water,f}$	95 °C	±0.7125 °C (±0.75% of reading)	
$T_{water,0}$	15 °C	±0.1125 °C (±0.75% of reading)	
T_a	21 °C	±0.1575 °C (±0.75% of reading)	
HV_{wood}	19,314kJ/kg	0	Commonly used value (Global Alliance for Clean Cookstoves 2014b)
HV_{char}	29,500 kJ/kg	0	Commonly used value (Global

			Alliance for Clean Cookstoves 2014b)
mc	0.09	±0.005	

The uncertainty equations for the megajoules of energy delivered to the pot (Eq. A.15) are shown below.

Equation	Value	Equation
$\frac{\partial MJ_d}{\partial m_{water,0}} = 0.000004197 * (T_{water,f} - T_{water,0} + 540.081)$	0.0025	Eq. A.18
$\frac{\partial MJ_d}{\partial T_{water,f}} = 0.000004197 * m_{water,0}$	0.02	Eq. A.19
$\frac{\partial MJ_d}{\partial T_{water,0}} = -0.000004197 * m_{water,0}$	-0.02	Eq. A.20
$\frac{\partial MJ_d}{\partial m_{water,f}} = -0.002257$	-0.02257	Eq. A.21
$\delta MJ_d = \sqrt{\left(\frac{\partial MJ_d}{\partial m_{water,0}} * \delta m_{water,0}\right)^2 + \left(\frac{\partial MJ_d}{\partial T_{water,f}} * \delta T_{water,f}\right)^2 + \left(\frac{\partial MJ_d}{\partial T_{water,0}} * \delta T_{water,0}\right)^2 + \left(\frac{\partial MJ_d}{\partial m_{water,f}} * \delta m_{water,f}\right)^2}$		
	0.01 MJ_d	Eq. A.22

The uncertainty of the megajoules of energy delivered to the pot is ±0.01 MJ. The uncertainty equations for the equivalent wood consumed (Eq. A.17) are shown below.

Equation	Value	Equation

$\frac{\partial m_{wood,eqv.}}{\partial m_{wood}} = \frac{HV_{wood} * (1 - mc) - \left(4.186 * mc * \left(T_{water,f} - T_a\right) + 2257\right)}{HV_{wood}}$	0.793	Eq. A.23
$\frac{\partial m_{wood,eqv.}}{\partial HV_{wood}} = \frac{m_{wood} * \left(4.186 * mc * \left(T_{water,f} - T_a\right) + 2257\right) + m_{char} * HV_{char}}{{HV_{wood}}^2}$	0.002	Eq. A.24
$\frac{\partial m_{wood,eqv.}}{\partial mc} = -\frac{\left(m_{wood} * \left(HV_{wood} + 4.186 * \left(T_{water,f} - T_a\right)\right)\right)}{HV_{wood}}$	-244.1	Eq. A.25
$\frac{\partial m_{wood,eqv.}}{\partial T_{water,f}} = -\frac{4.186 * m_{wood} * mc}{HV_{wood}}$	-0.0047	Eq. A.26
$\frac{\partial m_{wood,eqv.}}{\partial T_a} = \frac{4.186 * m_{wood} * mc}{HV_{wood}}$	0.0047	Eq. A.27
$\frac{\partial m_{wood,eqv.}}{\partial m_{char}} = -\frac{HV_{char}}{HV_{wood}}$	-1.527	Eq. A.28
$\frac{\partial m_{wood,eqv.}}{\partial HV_{char}} = -\frac{m_{char}}{HV_{wood}}$	-0.00026	Eq. A.29
$\delta m_{wood,eqv.} = \sqrt{\left(\frac{\partial m_{wood,eqv.}}{\partial m_{wood}} * \delta m_{wood}\right)^2 + \left(\frac{\partial m_{wood,eqv.}}{\partial HV_{wood}} * \delta HV_{wood}\right)^2 + \left(\frac{\partial m_{wood,eqv.}}{\partial mc} * \delta mc\right)^2 + \left(\frac{\partial m_{wood,eqv.}}{\partial T_{water,f}} * \delta T_{water,f}\right)^2 + \left(\frac{\partial m_{wood,eqv.}}{\partial T_a} * \delta T_a\right)^2 + \left(\frac{\partial m_{wood,eqv.}}{\partial m_{char}} * \delta m_{char}\right)^2 + \left(\frac{\partial m_{wood,eqv.}}{\partial HV_{char}} * \delta HV_{char}\right)^2}$	2.1 g	Eq. A.30

The uncertainty of the equivalent mass of wood consumed is ±2.1 g. The result of Eq. 17 is then used in Eq. 16 to calculate the megajoules produced. The uncertainty equations for the megajoules produced (Eq. A.16) are shown below.

Equation	Value	Equation
$\frac{\partial MJ}{\partial m_{wood,eqv.}} = \frac{HV_{wood}}{1000000}$	0.019314	Eq. A.31
$\frac{\partial MJ}{\partial HV_{wood}} = \frac{m_{wood,eqv.}}{1000000}$	0.00021	Eq. A.32
$\delta MJ = \sqrt{\left(\frac{\partial MJ}{\partial m_{wood,eqv.}} * \delta m_{wood,eqv.}\right)^2 + \left(\frac{\partial MJ}{\partial HV_{wood}} * \delta HV_{wood}\right)^2}$	0.04 MJ	Eq. A.33

The uncertainty of the megajoules of energy produced is ±0.04 MJ.

A.1.4 Particulate Matter Uncertainty

The global equation used to calculate the total $PM_{2.5}$ produced is as follows:

$$m_{PM2.5} = \frac{\left((m_f - m_0) * DL * Q\right)}{3 * 1000 * CF} \quad \text{Eq. A.34}$$

Where m_f and m_0 are the reported total masses from the TEOM at the end and start of the test, respectively (µg), DL is the calculated dilution ratio of the external dilution system, Q is the flow rate through the hood and ducting system (L/min), 3 is the flow rate required by the TEOM system in liters per minute, and CF is the calculated correction factor. The input variables and associated uncertainties are listed below.

Variable	Nominal Value	Uncertainty	Notes
m_f	111.2 µg/115 µg	±0.19 µg/±0.20 µg	Nominal value comes from real test. The two values are for Tier 4 high power/low power.
m_0	107.7 µg	±0.19 µg	Nominal value comes from real test
DL	18.75	±0.94	Uncertainty was measured over the course of recalibrations
FR	5097 L/min	±40.5 L/min	Uncertainty calculated in Section A.1.1
CF	1.49	±0.05	

The uncertainty equations for the total mass of $PM_{2.5}$ produced over the duration of a test (Eq. A.34) are shown below.

Equation	Value	Equation
$\frac{\partial m_{PM2.5}}{\partial m_f} = \frac{DL * Q}{3000 * CF}$	21.38	Eq. A.35
$\frac{\partial m_{PM2.5}}{\partial m_0} = -\frac{DL * Q}{3000 * CF}$	-21.38	Eq. A.36
$\frac{\partial m_{PM2.5}}{\partial DL} = \frac{Q * (m_f - m_0)}{3000 * CF}$	3.99/8.32	Eq. A.37
$\frac{\partial m_{PM2.5}}{\partial Q} = \frac{DL * (m_f - m_0)}{3000 * CF}$	0.015/0.031	Eq. A.38
$\frac{\partial m_{PM2.5}}{\partial CF} = -\frac{DL * Q * (m_f - m_0)}{3000 * CF^2}$	-50.22/-104.75	Eq. A.39
$\delta m_{PM2.5} = \sqrt{\left(\frac{\partial m_{PM2.5}}{\partial m_f} * \delta m_f\right)^2 + \left(\frac{\partial m_{PM2.5}}{\partial m_0} * \delta m_0\right)^2 + \left(\frac{\partial m_{PM2.5}}{\partial DL} * \delta DL\right)^2 + \left(\frac{\partial m_{PM2.5}}{\partial Q} * \delta Q\right)^2 + + \left(\frac{\partial m_{PM2.5}}{\partial CF} * \delta CF\right)^2}$	7.4 mg/11.2 mg	Eq. A.40

The uncertainty of the total mass of $PM_{2.5}$ produced over the duration of a test for Tier 4 high power PM is ±7.4 mg. The uncertainty of the total mass of $PM_{2.5}$ produced over the duration of a test for Tier 4 low power PM is ±11.2 mg. This is the uncertainty associated with Tier 4 high-power PM.

A.1.5 ISO/IWA Comparison Tiers Uncertainty

Uncertainties calculated in Sections A.1.1-A.1.4 were taken to calculate the overall uncertainties for each of the ISO/IWA comparison metrics. The ISO/IWA comparison metrics input variables along with the necessary calculation and relevant uncertainties are shown below.

ISO/IWA Metric	Calculation	Input Variables	Nominal Value	Uncertainty	Notes
High Power CO (g/MJ$_d$)	$CO_{HP} = \frac{g_{CO}}{MJ_d}$	g_{CO}	14 g	±0.9 g	Section A.1.2
		MJ_d	1.8 MJ	±0.01 MJ	Section A.1.3
Low Power CO (g/min/L)	$CO_{LP} = \frac{g_{CO}}{min * L}$	g_{CO}	14 g	±0.9 g	Nominal value assumes Tier 4, 3.5 L, and 45 minute simmer
		min	45 min	0	
		L	3.5 L	±0.001 L	Uncertainty determined by scale
High Power PM$_{2.5}$ (mg/MJ$_d$)	$PM_{HP} = \frac{mg_{PM}}{MJ_d}$	mg_{PM}	74.9 mg	±7.4 mg	Section A.1.4
		MJ_d	1.8 MJ	±0.01 MJ	Section A.1.3
Low Power PM$_{2.5}$ (mg/min/L)	$PM_{LP} = \frac{mg_{PM}}{min * L}$	mg_{PM}	157.5 mg	±11.2 mg	Nominal value assumes Tier 4, 3.5 L, and 45 minute simmer
		min	45 min	0	
		L	3.5 L	±0.001 L	Uncertainty determined by scale
High Power Thermal Efficiency (%)	$\eta_{HP} = \frac{MJ_d}{MJ}$	MJ_d	1.8 MJ	±0.01 MJ	Section A.1.3
		MJ	4 MJ	±0.04 MJ	Section A.1.3
Low Power Specific Consumption (MJ/L/min)	$\eta_{LP} = \frac{MJ}{min * L}$	MJ	2.7 MJ	±0.04 MJ	Nominal value assumes Tier 3, 3.5 L, and 45 minute simmer
		min	45 min	N/A	
		L	3.5 L	±0.001 L	Uncertainty determined by scale
Indoor Emissions CO	$IE_{CO} = \frac{g_{CO}}{min}$	g_{CO}	14 g	±0.9 g	Section A.1.2
		min	45 min	0	
		mg_{PM}	90 mg	±8 mg	Section A.1.4

Indoor Emissions $PM_{2.5}$	$IE_{PM} = \frac{mg_{PM}}{min}$	min	45 min	0	

The following calculations detail the uncertainty calculations for each ISO/IWA comparison tier.

They appear in the same order as shown above.

High power CO

Global equation:

$$CO_{HP} = \frac{g_{CO}}{MJ_d} \qquad \text{Eq. A.41}$$

Input variables and values:

Variable	Nominal Value	Uncertainty	Notes
g_{CO}	14 g	±0.9 g	Section A.1.2
MJ_d	1.8 MJ	±0.01 MJ	Section A.1.3

Uncertainty calculations:

Equation	Value	Equation
$\frac{\partial CO_{HP}}{\partial g_{CO}} = \frac{1}{MJ_d}$	0.56	Eq. A.42
$\frac{\partial CO_{HP}}{\partial MJ_d} = -\frac{g_{CO}}{MJ_d^2}$	-4.32	Eq. A.43
$\delta CO_{HP} = \sqrt{\left(\frac{\partial CO_{HP}}{\partial g_{CO}} * \delta g_{CO}\right)^2 + \left(\frac{\partial CO_{HP}}{\partial MJ_d} * \delta MJ_d\right)^2}$	0.50 g/MJ_d	Eq. A.44

Low power CO

Global equation:

$$CO_{LP} = \frac{g_{CO}}{min * L} \qquad \text{Eq. A.45}$$

Input variables and values:

Variable	Nominal Value	Uncertainty	Notes
g_{CO}	14 g	±0.9 g	Section A.1.2
min	45 min	0	
L	3.5 L	±0.001 L	Uncertainty determined by scale

Uncertainty calculations:

Equation	Value	Equation
$\frac{\partial CO_{LP}}{\partial g_{CO}} = \frac{1}{min * L}$	0.006	Eq. A.46
$\frac{\partial CO_{LP}}{\partial min} = -\frac{g_{CO}}{min^2 * L}$	-0.002	Eq. A.47
$\frac{\partial CO_{LP}}{\partial L} = -\frac{g_{CO}}{min * L^2}$	-0.025	Eq. A.48
$\delta CO_{LP} = \sqrt{\left(\frac{\partial CO_{LP}}{\partial g_{CO}} * \delta g_{CO}\right)^2 + \left(\frac{\partial CO_{LP}}{\partial min} * \delta min\right)^2 + \left(\frac{\partial CO_{LP}}{\partial L} * \delta L\right)}$	0.006 g/min/L	Eq. A.49

High power PM

Global equation:

$$PM_{HP} = \frac{mg_{PM}}{MJ_d} \qquad \text{Eq. A.50}$$

Input variables and values:

Variable	Nominal Value	Uncertainty	Notes
mg_{PM}	74.9 mg	±7.4 mg	Section A.1.4
MJ_d	1.8 MJ	±0.01 MJ	Section A.1.3

Uncertainty calculations:

Equation	Value	Equation
$\frac{\partial PM_{HP}}{\partial mg_{PM}} = \frac{1}{MJ_d}$	0.56	Eq. A.51
$\frac{\partial PM_{HP}}{\partial MJ_d} = -\frac{mg_{PM}}{MJ_d^2}$	-23.12	Eq. A.52
$\delta PM_{HP} = \sqrt{\left(\frac{\partial PM_{HP}}{\partial mg_{PM}} * \delta mg_{PM}\right)^2 + \left(\frac{\partial PM_{HP}}{\partial MJ_d} * \delta MJ_d\right)^2}$	4.1 mg/MJ_d	Eq. A.53

Low power PM

Global equation:

$$PM_{LP} = \frac{mg_{PM}}{min * L} \quad \text{Eq. A.54}$$

Input variables and values:

Variable	Nominal Value	Uncertainty	Notes
mg_{PM}	157.5 mg	±11.2 mg	Section A.1.4
min	45 min	0	
L	3.5 L	±0.001 L	Uncertainty determined by scale

Uncertainty calculations:

Equation	Value	Equation
$\frac{\partial PM_{LP}}{\partial mg_{PM}} = \frac{1}{min * L}$	0.006	Eq. A.55
$\frac{\partial PM_{LP}}{\partial min} = -\frac{mg_{PM}}{min^2 * L}$	-0.022	Eq. A.56
$\frac{\partial PM_{LP}}{\partial L} = -\frac{mg_{PM}}{min * L^2}$	-0.286	Eq. A.57
$\delta PM_{LP} = \sqrt{\left(\frac{\partial PM_{LP}}{\partial mg_{PM}} * \delta mg_{PM}\right)^2 + \left(\frac{\partial PM_{LP}}{\partial min} * \delta min\right)^2 + \left(\frac{\partial PM_{LP}}{\partial L} * \delta L\right)}$	0.07 mg/min/L	Eq. A.58

High power thermal efficiency

Global equation:

$$\eta_{HP} = \frac{MJ_d}{MJ} \qquad \text{Eq. A.59}$$

Input variables and values:

Variable	Nominal Value	Uncertainty	Notes
MJ_d	1.8 MJ	±0.01 MJ	Section A.1.3
MJ	4 MJ	±0.04 MJ	Section A.1.3

Uncertainty calculations:

Equation	Value	Equation
$\frac{\partial \eta_{HP}}{\partial MJ_d} = \frac{1}{MJ}$	0.25	Eq. A.60
$\frac{\partial \eta_{HP}}{\partial MJ} = -\frac{MJ_d}{MJ^2}$	-0.11	Eq. A.61
$\delta\eta_{HP} = \sqrt{\left(\frac{\partial \eta_{HP}}{\partial MJ_d} * \delta MJ_d\right)^2 + \left(\frac{\partial \eta_{HP}}{\partial MJ} * \delta MJ\right)^2}$	0.005	Eq. A.62

Low power specific consumption

Global equation:

$$\eta_{LP} = \frac{MJ}{min * L} \qquad \text{Eq. A.63}$$

Input variables and values:

Variable	Nominal Value	Uncertainty	Notes
MJ	2.7 MJ	±0.04 MJ	Nominal value assumes Tier 4, 3.5 L, and 45 minute simmer
min	45 min	0	
L	3.5 L	±0.001 L	Uncertainty determined by scale

Uncertainty calculations:

Equation	Value	Equation
$\frac{\partial \eta_{LP}}{\partial MJ} = \frac{1}{min * L}$	0.006	Eq. A.64
$\frac{\partial \eta_{LP}}{\partial min} = -\frac{MJ}{min^2 * L}$	-0.0004	Eq. A.65
$\frac{\partial \eta_{LP}}{\partial L} = -\frac{MJ}{min * L^2}$	-0.005	Eq. A.66
$\delta \eta_{LP} = \sqrt{\left(\frac{\partial \eta_{LP}}{\partial MJ} * \delta MJ\right)^2 + \left(\frac{\partial \eta_{LP}}{\partial min} * \delta min\right)^2 + \left(\frac{\partial \eta_{LP}}{\partial L} * \delta L\right)}$	0.0003 MJ/min/L	Eq. A.67

Indoor Emissions CO

Global equation:

$$IE_{CO} = \frac{g_{CO}}{min} \qquad \text{Eq. A.68}$$

Input variables and values:

Variable	Nominal Value	Uncertainty	Notes
g_{CO}	14 g	±0.9 g	Section A.1.2
min	45 min	0	

Uncertainty calculations:

Equation	Value	Equation
$\frac{\partial IE_{CO}}{\partial g_{CO}} = \frac{1}{min}$	0.022	Eq. A.69
$\frac{\partial IE_{CO}}{\partial min} = -\frac{g_{CO}}{min^2}$	-0.008	Eq. A.70
$\delta IE_{CO} = \sqrt{\left(\frac{\partial IE_{CO}}{\partial g_{CO}} * \delta g_{CO}\right)^2 + \left(\frac{\partial IE_{CO}}{\partial min} * \delta min\right)^2}$	0.02 g/min	Eq. A.71

Indoor Emissions PM

Global equation:

$$IE_{PM} = \frac{mg_{PM}}{min} \qquad \text{Eq. A.72}$$

Input variables and values:

Variable	Nominal Value	Uncertainty	Notes
mg_{PM}	90 mg	±8 mg	Section A.1.4
min	45 min	0	

Uncertainty calculations:

Equation	Value	Equation
$\frac{\partial IE_{PM}}{\partial mg_{PM}} = \frac{1}{min}$	0.022	Eq. A.73
$\frac{\partial IE_{PM}}{\partial min} = -\frac{mg_{PM}}{min^2}$	-0.04	Eq. A.74
$\delta IE_{PM} = \sqrt{\left(\frac{\partial IE_{PM}}{\partial mg_{PM}} * \delta mg_{PM}\right)^2 + \left(\frac{\partial IE_{PM}}{\partial min} * \delta min\right)^2}$	0.18 mg/min	Eq. A.75

A.2 Bernoulli's Equation Applied to Cookstoves

Bernoulli's equation can be used to give a very rough estimation of the flow rates through a stove. As applying Bernoulli's equation to complex geometries such as those found in cookstoves is difficult, these calculations are used to provide general mechanistic explanations of observed behaviors. One such example is using Bernoulli's equation to understand how the flow rates through a cookstove vary as firepower increases. Bernoulli's equation,

$$P_1 + \frac{1}{2}\rho_1 v_1^2 + \rho_1 g h_1 = P_2 + \frac{1}{2}\rho_2 v_2^2 + \rho_2 g h_2 \qquad \text{Eq. A.76}$$

where the subscripts 1 and 2 denote the entrance and exit conditions, can simplified by negating the two pressure terms due to the insignificant change in pressure and by negating the initial velocity term, as the ambient velocity is near zero. The equation can then be rearranged to solve for the exit velocity, v_2.

$$v_2 = \sqrt{\frac{2(\rho_1 - \rho_2)h}{\rho_2}} \qquad \text{Eq. A.77}$$

The densities (ρ_1 and ρ_2) are calculated using the ideal gas law. The exit gas temperature used to calculate ρ_2 is varied over a range of typically seen temperatures during testing, measured using a thermocouple (500-950 K). The entrance temperature is assumed to be 300 K. The height is kept at 0.3 m. The exit velocity is then used to calculate the mass flow rate, using the exit density and cross-sectional flow area of the stove, shown in Eq. A.78.

$$\dot{m} = v_2 * A * \rho_2 \qquad \text{Eq. A.78}$$

References

1. Aleixandre, M.; Gerboles, M. Review of Small Commercial Sensors for Indicative Monitoring of Ambient Gas. *Chemical Engineering Transactions*. 2012, 30.
2. Alonso, M.; Kousaka, Y. Mobility Shift in the Differential Mobility Analyzer Due to Brownian Diffusion and Space-Charge Effects. *Journal of Aerosol Science*. 1996, *27*, 1201–1225.
3. Aprovecho Research Center. *Instructions for Use of the Laboratory Emissions Monitoring System (LEMS).* 2013.
4. Berrueta, V. M.; Edwards, R. D.; Masera, O. R. Energy Performance of Wood-Burning Cookstoves in Michoacan, Mexico. *Renewable Energy*. 2008, *33*, 859–870.
5. Bjornsson, S.; Novosselov, I. Advanced Control Methodology for Biomass Combustion. Thesis, University Of Washington, 2014.
6. Bond, T. C.; Streets, D. G.; Yarber, K. F.; Nelson, S. M.; Woo, J.; Klimont, Z. A technology-based global inventory of black and organic carbon emissions from combustion. *J. Geophys. Res. 2004, 109*, D14203.
7. Bond, T. C.; Sun, H. Can Reducing Black Carbon Emissions Counteract Global Warming? *Environmental Science & Technology Environ. Sci. Technol.* 2005, *39*, 5921–5926.
8. Bonjour, S.; Adair-Rohani, H.; Wolf, J.; Bruce, N. G.; Mehta, S.; Prüss-Ustün, A.; Lahiff, M.; Rehfuess, E. A.; Mishra, V.; Smith, K. R. Solid Fuel Use For Household Cooking: Country and Regional Estimates for 1980–2010. *Environ. Health Perspect. Environmental Health Perspectives*. 2013, *121*, 784–790.
9. Chen, D.; Pui, D. Y.; Hummes, D.; Fissan, H.; Quant, F.; Sem, G. Nanometer Differential Mobility Analyzer (Nano-DMA): Design and Numerical Modeling. *Journal of Aerosol Science*. 1996, *27*.

10. Chen, Y.; Roden, C. A.; Bond, T. C. Characterizing Biofuel Combustion With Patterns of Real-Time Emission Data (PaRTED). *Environmental Science & Technology Environ. Sci. Technol.* 2012, *46*, 6110–6117.
11. Cyrys, J.; Dietrich, G.; Kreyling, W.; Tuch, T.; Heinrich, J. PM2.5 Measurements in Ambient Aerosol: Comparison between Harvard Impactor (HI) and the Tapered Element Oscillating Microbalance (TEOM) System. *Science of The Total Environment*. 2001, *278*, 191–197.
12. Edwards, R.; Smith, K. R.; Kirby, B.; Allen, T.; Litton, C. D.; Hering, S. An Inexpensive Dual-Chamber Particle Monitor: Laboratory Characterization. *Journal of the Air & Waste Management Association*. 2006, *56*, 789–799.
13. Ezzati, M.; Kammen, D. M. Quantifying The Effects of Exposure to Indoor Air Pollution from Biomass Combustion on Acute Respiratory Infections in Developing Countries. *Environmental Health Perspectives*. 2001, *109*, 481–488.
14. Fox, J. *An R And S-Plus Companion to Applied Regression*; Sage Publications: Thousand Oaks, CA, 2002.
15. Global Alliance for Clean Cookstoves. *Clean Cooking is Critical to Addressing Climate Change*. 2015.
16. Global Alliance for Clean Cookstoves. *Controlled Cooking Test (CCT).* 2004.
17. Global Alliance for Clean Cookstoves. *Kitchen Performance Test (KPT).* 2007.
18. Global Alliance for Clean Cookstoves. *The Water Boiling Test Version 4.2.3*. 2014a.
19. Global Alliance for Clean Cookstoves. *WBT 4.2.4 Spreadsheet.* 2014b
20. Green, D. C.; Fuller, G. W.; Baker, T. Development And Validation of the Volatile Correction Model for PM10 – An Empirical Method for Adjusting TEOM Measurements for Their Loss of Volatile Particulate Matter. *Atmospheric Environment*. 2009, *43*, 2132–2141.

21. Hahn, D. W. Light scattering theory, Department of Mechanical and Aerospace Engineering, University of Florida. 2004
22. Hauck, H.; Berner, A.; Gomiscek, B.; Stopper, S.; Puxbaum, H.; Kundi, M.; Preining, O. On The Equivalence of Gravimetric PM Data with TEOM and Beta-Attenuation Measurements. *Journal of Aerosol Science*. 2004, *35*, 1135–1149.
23. Hinds, W. C. *Aerosol Technology: Properties, Behavior, and Measurement of Airborne Particles*; J. Wiley: New York, 1982.
24. Hutton, G.; Rehfuess, E.; Tediosi, F. *Energy for Sustainable Development*. 2007, *11* (4), 34–43.
25. ISO. *IWA 11:2012: Guidelines for evaluating cookstove performance*. 2012. Available: http://www.iso.org/iso/catalogue_detail?csnumber=61975
26. Jetter, J.; Zhao, Y.; Smith, K. R.; Khan, B.; Yelverton, T.; Decarlo, P.; Hays, M. D. Pollutant Emissions And Energy Efficiency under Controlled Conditions for Household Biomass Cookstoves and Implications for Metrics Useful in Setting International Test Standards. *Environmental Science & Technology Environ. Sci. Technol.* 2012, *46*, 10827–10834.
27. Johnson, M.; Edwards, R.; Berrueta, V.; Masera, O. New Approaches To Performance Testing of Improved Cookstoves. *Environmental Science & Technology Environ. Sci. Technol.* 2010, *44*, 368–374.
28. Johnson, M.; Edwards, R.; Frenk, C. A.; Masera, O. In-Field Greenhouse Gas Emissions from Cookstoves in Rural Mexican Households. *Atmospheric Environment*. 2008, *42*, 1206–1222.
29. Just, B.; Rogak, S.; Kandlikar, M. Characterization Of Ultrafine Particulate Matter from Traditional and Improved Biomass Cookstoves. *Environmental Science & Technology Environ. Sci. Technol.* 2013, 130319140434009.

30. Kobayashi N.; Okada N.; Hirakawa, A.; Sato, T.; Kobayashi, J.; Hatano, S.; Itaya, Y.; Mori, S.: Characteristics of solid residues obtained from hot-compresses-water treatment of woody biomass. *Industrial & Engineering Chemistry Research*. 2009, 48, 373-379.
31. Kshirsagar, M. P.; Kalamkar, V. R. A Comprehensive Review on Biomass Cookstoves and a Systematic Approach for Modern Cookstove Design. *Renewable and Sustainable Energy Reviews*. 2014, *30*, 580–603.
32. Lamlom, S.; Savidge, R. A Reassessment of Carbon Content in Wood: Variation within and between 41 North American Species. *Biomass and Bioenergy*. 2003, *25*, 381–388.
33. L'orange, C.; Defoort, M.; Willson, B. Influence Of Testing Parameters on Biomass Stove Performance and Development of an Improved Testing Protocol. *Energy for Sustainable Development*. 2012, *16*, 3–12.
34. Maccarty, N.; Still, D.; Ogle, D. Fuel Use and Emissions Performance of Fifty Cooking Stoves in the Laboratory and Related Benchmarks of Performance. *Energy for Sustainable Development*. 2010, *14*, 161–171.
35. MacCarty, N.; Still, D.; Ogle, D.; Drouin, T. Assessing cook stove performance: field and lab studies of three rocket stoves comparing the open fire and traditional stoves in Tamil Nadu, India on measures of time to cook, fuel use, total emissions, and indoor air pollution. *Aprovecho Research Center*. 2008.
36. Manibog, F. R. Improved Cooking Stoves In Developing Countries: Problems and Opportunities. *Annu. Rev. Energy. Annual Review of Energy*. 1984, *9*, 199–227.
37. Masera, O.; Edwards, R.; Arnez, C. A.; Berrueta, V.; Johnson, M.; Bracho, L. R.; Riojas-Rodríguez, H.; Smith, K. R. Impact Of Patsari Improved Cookstoves on Indoor Air Quality in Michoacán, Mexico. *Energy for Sustainable Development*. 2007, *11*, 45–56.
38. Mccracken, J.; Smith, K. Emissions And Efficiency of Improved Woodburning Cookstoves in Highland Gatemala. *Environment International*. 1998, *24*, 739–747.

39. Mohankumar, D.; Vanderlick, F.; McGee, R.; Parnell, C.; Auvermann, B.; Lambeth, B.; Skloss, S. Comparison of TEOM and Gravimetric Methods of Measuring PM Concentrations. *Journal of Natural and Environmental Sciences.* 2011, *2*, 19-24.
40. Molenar, J. V. *Theoretical analysis of PM2.5 mass measurements by nephelometry - #110*; tech.; 2005.
41. Meyer, N. K.; Lauber, A.; Nussbaumer, T.; Burtscher, H. Influence Of Particle Charging on TEOM Measurements in the Presence of an Electrostatic Precipitator. *Atmos. Meas. Tech. Discuss. Atmospheric Measurement Techniques Discussions*. 2008, *1*, 435–449.
42. Pandey, S. K.; Kim, K.-H. The Relative Performance Of NDIR-Based Sensors in the Near Real-Time Analysis of CO2 in Air. *Sensors*. 2007, *7*, 1683–1696.
43. Posada, D.; Buckley, T. Model Selection And Model Averaging in Phylogenetics: Advantages of Akaike Information Criterion and Bayesian Approaches Over Likelihood Ratio Tests. *Systematic Biology*. 2004, *53*, 793–808.
44. Rockne, K. J.; Taghon, G. L.; Kosson, D. S. Pore Structure of Soot Deposits from Several Combustion Sources. *Chemosphere*. 2000, *41*, 1125–1135.
45. Roden, C. A.; Bond, T. C.; Conway, S.; Pinel, A. B. O.; Maccarty, N.; Still, D. Laboratory And Field Investigations of Particulate and Carbon Monoxide Emissions from Traditional and Improved Cookstoves. *Atmospheric Environment*. 2009, *43*, 1170–1181.
46. Santos, J. P.; Hontañón, E.; Ramiro, E.; Alonso, M. Performance Evaluation of a High-Resolution Parallel-Plate Differential Mobility Analyzer. *Atmospheric Chemistry and Physics Atmos. Chem. Phys.* 2009, *9*, 2419–2429.
47. Schwartz, J.; Dockery, D. W.; Neas, L. M. Is Daily Mortality Associated Specifically With Fine Particles? *Journal of the Air & Waste Management Association*. 1996, *46*, 927–939.
48. Smith, K. R.; Dutta, K.; Chengappa, C.; Gusain, P.; Berrueta, O. M. A. V.; Edwards, R.; Bailis, R.; Shields, K. N. Monitoring And Evaluation of Improved Biomass Cookstove Programs for Indoor Air Quality and Stove Performance: Conclusions from the

Household Energy and Health Project. *Energy for Sustainable Development*. 2007, *11*, 5–18.

49. ThermoFisher Scientific. *Operating Guide, TEOM 1405*; 2008.
50. Thomas, A.; Gebhart, J. Correlations Between Gravimetry and Light Scattering Photometry for Atmospheric Aerosols. *Atmospheric Environment*. 1994, *28*, 935–938.
51. United Kingdom Department for Environment, Food and Rural Affairs. *The Air Quality Strategy for England, Scotland, Wales and Northern Ireland Volume 2*; 2007.
52. United States Environmental Protection Agency. *Method 5 - Particulate Matter (PM)*.
53. Vega, E.; Reyes, E.; Wellens, A.; Sánchez, G.; Chow, J.; Watson, J. Comparison Of Continuous and Filter Based Mass Measurements in Mexico City. *Atmospheric Environment*. 2003, *37*, 2783–2793.
54. Wanjura, J. D.; Shaw, B. W.; Parnell, C. B.; J.; Lacey, R. E.; Capareda, S. C. Comparison Of Continuous Monitor (TEOM) and Gravimetric Sampler Particulate Matter Concentrations. *Transactions of the ASABE*. 2008, *51*, 251–257.
55. Weiden, S.-L. V. D.; Drewnick, F.; Borrmann, S. Particle Loss Calculator – a New Software Tool for the Assessment of the Performance of Aerosol Inlet Systems. *Atmos. Meas. Tech. Atmospheric Measurement Techniques*. 2009, *2*, 479–494.
56. Willeke, K.; Baron, P. A. *Aerosol Measurement: Principles, Techniques, and Applications*; Van Nostrand Reinhold: New York, 1993.
57. World Health Organization. *Air Quality Guidelines Global Update - 2005. Particulate Matter, Ozone, Nitrogen Dioxide, and Sulfur Dioxide*. 2006.
58. World Health Organization. *Burden of disease from Household Air Pollution for 2012*. 2014.
59. World Health Organization. *WHO Guidelines for Indoor Air Quality: Household Fuel Combustion.* 2014.